

Boltzmann Machine Learning and Regularization Methods for Inferring Evolutionary Fields and Couplings from a Multiple Sequence Alignment

Sanzo Miyazawa

Abstract—The inverse Potts problem to infer a Boltzmann distribution for homologous protein sequences from their single-site and pairwise amino acid frequencies recently attracts a great deal of attention in the studies of protein structure and evolution. We study regularization and learning methods and how to tune regularization parameters to correctly infer interactions in Boltzmann machine learning. Using L_2 regularization for fields, group L_1 for couplings is shown to be very effective for sparse couplings in comparison with L_2 and L_1 . Two regularization parameters are tuned to yield equal values for both the sample and ensemble averages of evolutionary energy. Both averages smoothly change and converge, but their learning profiles are very different between learning methods. The Adam method is modified to make stepsize proportional to the gradient for sparse couplings. It is shown by first inferring interactions from protein sequences and then from Monte Carlo samples that the fields and couplings can be well recovered, but that recovering the pairwise correlations in the resolution of a total energy is harder for the natural proteins than for the protein-like sequences. Selective temperature for folding/structural constrains in protein evolution is also estimated.

Index Terms—group L_1 , inverse Potts problem, learning method, optimum regularization, sparse interactions, selective temperature.

1 INTRODUCTION

THE maximum entropy model, $P(\sigma) \propto \exp(-\psi_N(\sigma))$, where $\psi_N \equiv -[\sum_i \{h_i(\sigma_i) + \sum_{j>i} J_{ij}(\sigma_i, \sigma_j)\}]$, sequence $\sigma \equiv (\dots, \sigma_i, \dots)$, and $\sigma_i \in \{\text{amino acids, deletion}\}$, for the distribution of homologous proteins in sequence space recently attracts a great deal of attention in particular due to its capacity to accurately predict residue-residue contacts in a 3D protein structure and complex [1], [2], [3], [4], [5], [6], [7]. Because genome-wide analyses require computationally fast methods, approximate methods such as the mean field approximation [1], [2], [8], [9] and pseudo-likelihood maximization methods [10], [11] have been employed for the inverse Potts problem that is to infer fields ($h_i(a_k)$) and couplings ($J_{ij}(a_k, a_l)$) from single-site frequencies, $P_i(a_k)$ where $a_k \in \{\text{amino acids, deletion}\}$, and pairwise frequencies, $P_{ij}(a_k, a_l)$, observed in a multiple sequence alignment (MSA); see methods S.1.1 of the supplementary material. The performance of contact prediction by the mean-field or pseudo-likelihood maximization method is sufficiently good [4], but it has been reported [12], [13], [14] that these methods can recover the structure of the interaction network but typically not the correct strength of interactions. The estimates of the fields and couplings are also employed, however, to discuss protein evolution [15], [16], particularly to analyze coevolution between residue substitutions, and to discuss protein folding [17], [18]. Unlike contact predictions, accurate estimations of the fields and couplings are required in these studies; for instance, quantitative analyses of the effects of amino acid substitutions on protein stability, which are also discussed in this manuscript. One of generative methods that can better recover sequence statistics [12], [13], [14] is a Boltzmann machine learning (BML) [19], [20], [21], [22], in which pairwise

marginal distributions are estimated by Markov chain Monte Carlo (MCMC) samplings with the Metropolis-Hastings algorithm [23], [24] or Gibbs sampler [25], and the fields and couplings are iteratively inferred by maximizing log-likelihood, equivalently by minimizing cross entropy; see methods S.1.6.

The number of parameters, fields and couplings, to be optimized in the inverse Potts problem is very large in comparison with learning data. To prevent over-fitting, regularization terms are often employed as part of the objective function. Including the regularization terms in the cross entropy also fixes the gauge for the evolutionary potential $\psi_N(\sigma)$, which is gauge-invariant, that is, invariant under a certain transformation of fields and couplings; see methods S.1.9. An appropriate regularization model and hyper-parameters, however, must be employed to correctly infer fields and couplings. Also, a learning method must be one leading to reasonable values for fields and couplings. However, problems are: 1) Natural proteins with known fields and couplings are not available to optimize hyper-parameters and to choose a better regularization model and gradient-descent method. 2) In addition, in the Boltzmann machine (BM) the learning process fluctuates, but the cross entropy/likelihood cannot be used to pick up the best set of parameters, because it can hardly be evaluated, even though its partial derivatives can be easily evaluated.

Then, what characteristics are required for the fields and couplings in protein sequences? 1) Couplings (J_{ij}) should be sparse and their strength is expected to negatively correlate with the distance between residues, because strong residue-residue correlations/coevolutions are expected for closely-located, interacting residue pairs in a 3D protein structure and complex [1], [2], [8], [9], [22], [26], [27], [28], [29], [30], [31], [32], [33], [34], [35], [36], [37], [38], [39], [40], [41], [42], [43], [44], [45], [46], [47], [48], [49], although weak coevolutions may occur to select less-attractive residue pairs for distantly-located residue pairs [17]. 2) The sample mean of $\psi_N(\sigma) \equiv -[\sum_i \{h_i(\sigma_i) + \sum_{j>i} J_{ij}(\sigma_i, \sigma_j)\}]$

• Email: sanzo.miyazawa@gmail.com

Manuscript received 20 Sept. 2019; revised 8 Apr. 2020; accepted 2 May 2020; DOI: 10.1109/TCBB.2020.2993232 ; The corrections made afterward are indicated in red.

over homologous sequences $\sigma (= \sigma_N)$ is equal to the ensemble average over the Boltzmann distribution, which may be evaluated by approximating the distribution of $\psi_N(\sigma)$ of random sequences as a Gaussian distribution, $\bar{\psi} - \delta\psi^2$, where the $\bar{\psi}$ and $\delta\psi^2$ are the mean and variance of $\psi_N(\sigma)$ expected for the random sequences with the same amino acid composition [16], [50], [51], [52], [53]; see methods S.1.2 and methods S.1.3. In contact prediction, hyper-parameters have been optimized by maximizing the precision of contact prediction. However, the second requirement for fields and couplings above should be also satisfied by any method, if the evolutionary energies of natural sequences can be approximated to be at equilibrium in the Boltzmann distribution.

In the Boltzmann machine, statistical errors cannot be avoided in the estimation of the partial derivatives of cross entropy/log-likelihood, because they are evaluated on the basis of the pairwise marginal distributions estimated by MCMC samplings. As a result, even though the learning rate is sufficiently small, the cross entropy/log-likelihood are not expected to be monotonically improved but to fluctuate in the minimization/maximization process. In the present case, in which the first-order methods based on gradients are employed, the objective function will further fluctuate. Here, the average (D_2^{KL}) of the Kullback-Leibler divergences for pairwise marginal distributions over all residue pairs is monitored as an approximate measure of fitting to the target distribution. Although D_2^{KL} significantly fluctuates, the sample and ensemble averages of evolutionary energy along a learning process smoothly change and converge, but their profiles are very different between the learning methods, indicating which method is better than the others.

It is well-known that L_1 regularization is better for a sparse-parameter system than L_2 . In the present system, the couplings J must be sparse in terms of residue pair (i, j) . Hence, L_2 for the fields and group L_1 for the couplings (L2-GL1) are employed, and it is shown that the L2-GL1 model makes the estimate of the couplings more reasonable than the other models, L_2 for fields and L_1 for couplings (L2-L1) and L_2 for both (L2-L2); in the present work, the L1 for couplings means the elastic net including a small contribution of L_2 in addition to the L_1 regularization, because it is known [54] that the regularization of pure L_1 can occasionally produce non-unique solutions; see methods S.1.7.

Secondly, we show that it is preferable for the stepsize of parameter updates to be proportional to the partial derivative of the objective function, on estimating the dependencies of couplings J_{ij} on the distance between residues i and j . Various stochastic gradient-descent methods to minimize loss functions have been invented for machine learning; the momentum method [55], and Nesterov's Accelerated Momentum (NAG) (Fast proximal gradient method) [56] that manipulate the learning rate equally for all parameters, and AdaGrad [57], AdaDelta [58], RPROP [59], [60], RMSprop [61], and Adam [62] that employ adaptive learning rates for each parameter. The per-parameter adaptive learning rate methods, particularly Adam method, are ones that are often used in neural networks. They are stable and fast methods for stochastic gradient-descent. In the RPROP, a stepsize does not depend on the partial derivative but only on the temporal behavior of its sign. In the other per-parameter adaptive learning rate methods, a stepsize is proportional to the partial derivative but each partial derivative is normalized in such a way that stepsizes for all parameters are essentially a similar order. This characteristic of stepsizes appears to be inappropriate for the present case in which couplings are expected to be very sparse

and to correlate with residue-residue distance. For the present Potts problem, the RPROP method was modified [12], [14] in such a way that a stepsize is proportional to the partial derivative with the proportional constant determined by the RPROP method; we call this modified RPROP method RPROP-LR; the RPROP-LR stands for resilient propagation learning rate. Also, we invent and employ the modified Adam (ModAdam) method, in which the stepsize of parameter updates is proportional to the partial derivative, and the proportional constant is not per-parameter but adaptive; see methods S.1.8. Couplings inferred by the Adam, NAG, and RPROP-LR in the L2-L2 regularization model are compared with those by the ModAdam to show that the stepsize of parameter updates must be proportional to the partial derivative in order to better estimate the dependencies of couplings J_{ij} on the distance between residues i and j .

Thirdly, we discuss how to tune regularization parameters. In the present model, hyper-parameters that directly affect the estimates of fields and couplings are two proportional constants, λ_1 and λ_2 , for their regularization terms. These hyper-parameters are tuned in such a way that the sample mean of $\psi_N(\sigma_N)$ over homologous sequences σ_N is equal to $\bar{\psi} - \delta\psi^2$, where the $\bar{\psi}$ and $\delta\psi^2$ are the mean and variance of $\psi_N(\sigma)$ for the random sequences with the same amino acid composition.

By the L2-GL1 model and the ModAdam method, single-site frequencies and pairwise correlations can be well recovered. Also, by first estimating fields and couplings from protein sequences and then again from MCMC samples obtained by the Boltzmann machine learning, we show that fields and couplings in protein-like sequences can be well recovered, too. However, the distribution of evolutionary energies over natural proteins is shifted towards lower energies from that of MCMC samples, indicating that recovering the pairwise amino acid frequencies in the resolution of a total energy is harder for the natural proteins than for the protein-like sequences.

Lastly, based on the present estimates of fields and couplings, the constancy of the standard deviation of evolutionary energy changes due to single nucleotide nonsynonymous substitutions over protein families, which was found [16] by the mean field method, is confirmed. Then, selective temperature, which quantifies how strong the folding/structural constraints are in the evolution of a protein family [15], [16], [63], is estimated based on the evolutionary energy changes due to single amino acid substitutions [16]; see methods S.1.4 and S.1.5 for details.

Methods are described in detail in the supplementary file.

2 RESULTS

The multiple sequence alignments (MSA) of the Pfam [64], protein families PF00153 [14] and PF00595 [16], which include at least one member whose atomic coordinates are available, are only employed here, because of intensive computation, in order to demonstrate what regularization model and what type of gradient-descent method are preferable, how to tune regularization parameters, and how well the fields and couplings of protein-like sequences can be reproduced.

The protein family PF00595 (PDZ domain), which is a common structural domain of 80-90 amino-acids found in diverse signaling proteins, is chosen because experimental data of 31 folding free energy changes ($\Delta\Delta G_{ND}$) due to various types of single amino acid changes at many sites is available, which are required to estimate selective temperatures defined in Eq.

S12. On the other hand, PF00153 (Mitochondrial substrate/solute carrier) that consists of more family members than PF00595 has been chosen to examine the effects of alignment depth on the recoverability of single-site and pairwise amino acid frequencies and the estimation of fields and couplings.

The length of the proteins, the number of sequences (N) in the MSAs and their effective number (N_{eff}) are listed in Table 1. The number of sequences (M) that do not contain deletions and their effective number (M_{eff}) are also listed in this table as well as the PDB IDs of the protein structures employed to calculate contacting residue pairs.

TABLE 1
Protein Families Employed.

Pfam ID	N / N_{eff}^a	M^b / M_{eff}^a	L^c	PDB ID
PF00595 [†]	13814 / 4748.8	1255 / 340.0	81	1GM1-A:16-96
PF00153	54582 / 19473.9	255 / 139.8	97	2LCK-A:112-208

[†] Identical sequences are removed.

^a The effective number of sequences, $\sum_{\sigma_N} w_{\sigma_N}$, where the sample weight w_{σ_N} for a natural sequence σ_N is equal to the inverse of the number of sequences that are less than 20% different from a given sequence.

^b The number of unique sequences that include no deletion for PF00595 and no more than 2 for PF00153.

^c The number of residues in a sequence.

2.1 A Markov Chain Monte Carlo (MCMC) Method

Multiple Markov chains from different initial configurations with the same potential are generated by the Metropolis-Hastings algorithm [23], [24] in parallel computation and Markov chain Monte Carlo (MCMC) samplings are done in each chain to estimate pairwise marginal distributions after the fluctuation of $\psi_N(\sigma)$ passes a statistical test for an equilibrium condition. The Metropolis-Hastings algorithm was employed due to less computation time rather than the Gibbs sampler [25]. Then, the partial derivatives of the cross entropy including the regularization terms are evaluated according to Eqs. S40 and S41, and it is iteratively minimized by a gradient-descent method. The estimates of the partial derivatives on the basis of the marginal distributions estimated by the MCMC samplings strongly depend on the number of samples employed. The more samples are employed, the more precisely they can be estimated, although computational loads also increase. In the present case, the target frequencies are estimated from the MSA consisting of a limited number of sequences, limiting the accuracy of fields and couplings inferred. Employing too many samples to estimate marginal probabilities would cause over-fitting. Here, we employ samples whose number is equal to the effective number of sequences in the MSA in order to estimate the pairwise marginal distributions; $N_{\text{MC}} \approx N_{\text{eff}}$.

Because the first-order methods based on gradients are used for minimization, and also the estimates of the gradients include statistical errors due to MCMC samplings, the cross entropy including the regularization terms fluctuates during the process of the minimization. However, an optimum set of fields and couplings cannot be chosen on the basis of the cross entropy, because the cross entropy itself can hardly be evaluated although its partial derivatives can be. Here, the average of the Kullback-Leibler divergences of the pairwise marginal distributions over all site pairs is employed as an approximate measure of fitting to the target distribution; see Eq. S70.

2.2 How to Tune Regularization Parameters, λ_1 and λ_2

Hyper-parameters that directly affect the estimated values of parameters are two regularization parameters, λ_1 for fields $\phi_i(a_k)$ and λ_2 for couplings $\phi_{ij}(a_k, a_l)$; see Eqs. S46 and S54.

These parameters are tuned for inferred fields and couplings to satisfy the condition that the sample mean $\psi_N(\sigma_N)$ of evolutionary energies over homologous sequences σ_N is equal to the ensemble average $\langle \psi_N(\sigma) \rangle_{\sigma}$ of evolutionary energy in the Boltzmann distribution; according to the random energy model for protein folding [50], [51], [52], [53], the ensemble average is evaluated to be $\langle \psi_N(\sigma) \rangle_{\sigma} = \bar{\psi} - \delta\psi^2$ by approximating the distribution of the evolutionary energies of random sequences as a Gaussian distribution, where its mean ($\bar{\psi}$) and variance ($\delta\psi^2$) are evaluated to be equal to those of $\psi_N(\sigma)$ expected for random sequences whose amino acid composition is equal to the average amino acid composition of sequences in the MSA [16]; see Eqs. S6 and S9.

Increasing λ_1 and λ_2 enforces the values of $\phi_i(a_k)$ and $\phi_{ij}(a_k, a_l)$ toward zero, respectively. First, reduce the regularization terms by decreasing λ_1 with $\lambda_2 = \lambda_1$. The more it is reduced, the better single-site and pairwise probabilities become recovered. If λ_1 is reduced beyond a certain value, they will be over-fitted. In Fig. 1, $\psi_N(\sigma_N)$ and $\langle \psi_N(\sigma) \rangle_{\sigma}$ are plotted against λ_1 with $\lambda_2 = \lambda_1$. Energies are expressed in the Ising gauge for comparison; see Eq. S72. The ensemble average of evolutionary energy in the Gaussian approximation as well as the average evolutionary energy of homologous sequences in the MSA would decrease to favor those sequences as the regularization terms are reduced. At the certain value of λ_1 , where the over-fitting begins to occur, $\langle \psi_N(\sigma) \rangle_{\sigma}$ and $\psi_N(\sigma_N)$ almost take their minima. This value $\lambda_{1,0}$ is the optimum value for λ_1 . In the case of PF00153 that consists of more sequences than PF00595, $\psi_N(\sigma_N)$ is more negative than $\langle \psi_N(\sigma) \rangle_{\sigma}$, indicating that the natural sequences are over-favored. In the case of PF00595, they are almost equal to each other at the $\lambda_1 = \lambda_2 = \lambda_{1,0}$.

Then, increase λ_2 fixing λ_1 at $\lambda_1 = \lambda_{1,0}$. Increasing λ_2 increases sparsity in couplings, reducing coupling interactions including noises. As a result, the average evolutionary energy of homologous sequences in the MSA as well as the ensemble average of evolutionary energy in the Gaussian approximation would increase, and the former would become higher than the latter, because reducing couplings makes the target sequences unfavorable. A crossing point $\lambda_{2,0}$ of $\langle \psi_N(\sigma) \rangle_{\sigma}$ and $\psi_N(\sigma_N)$ is the optimum value for λ_2 , where the over-fitting disappears. The values of the regularization parameters determined in this way are listed in Table 2 for PF00595 and Table 3 for PF00153. These tables include those for the L2-GL1, L2-L2, and L2-L1 models.

In the case of employing the Monte Carlo samples obtained in Boltzmann machines as protein-like sequences, as the λ_1 is decreased below a certain value $\lambda_{1,0}$ with $\lambda_2 = \lambda_1$, $\langle \psi_N(\sigma) \rangle_{\sigma}$ becomes more negative than $\psi_N(\sigma)$, before both take their minima, because the average evolutionary energy of the Monte Carlo samples is much higher than that of the natural sequences as discussed later; this $\lambda_{1,0}$ is taken as the optimum value for λ_1 .

2.3 Dependences of Inferred Parameters on the Gradient-Descent Methods

First, the dependences of inferred parameters on the gradient-descent methods, Adam [62], NAG [56], RPROP-LR [12], [14], and ModAdam, are examined on PF00595; see methods S.1.8.

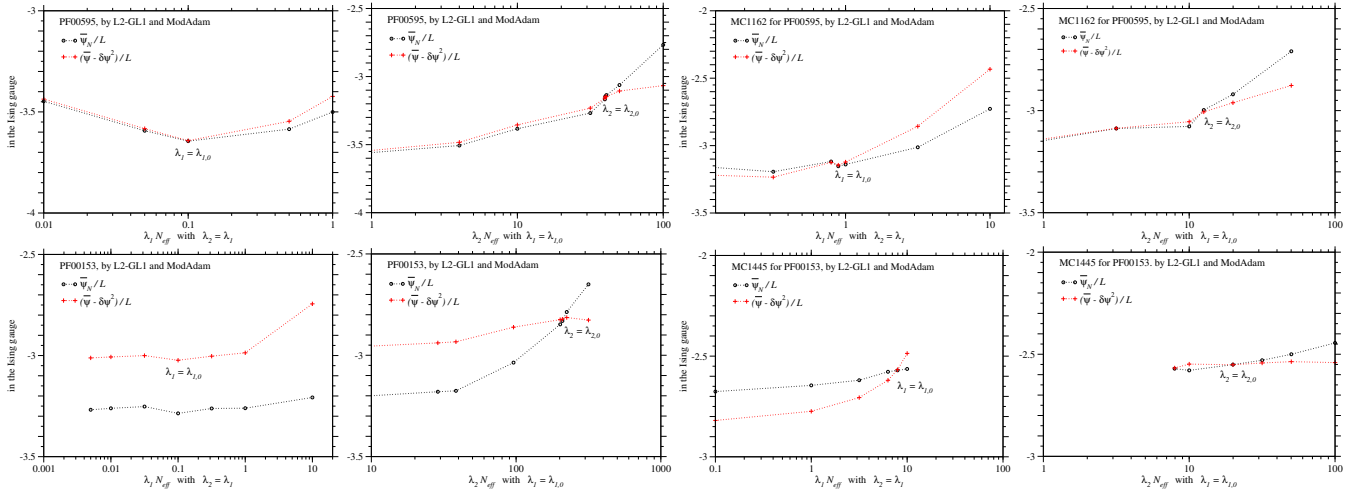


Fig. 1. A schematic representation of how to tune regularization parameters, λ_1 for fields and λ_2 for couplings. The average evolutionary energy per residue $\overline{\psi}_N/L$ of natural sequences and the ensemble average of evolutionary energy per residue $(\overline{\psi} - \delta\psi^2)/L$ in the Ising gauge are plotted by circle and plus marks, respectively, against one of the regularization parameters, $\lambda_1 N_{eff}$ with $\lambda_2 = \lambda_{1,0}$ and $\lambda_{2,0}$ are the optimum values of λ_1 and λ_2 , respectively. The regularization model L2-GL1 and the modified Adam method are employed; see Tables 2 and 3 for the values of $\lambda_{1,0}$ and $\lambda_{2,0}$. The upper and lower rows correspond to the figures for PF00595 and PF00153, respectively. The left four figures are for natural sequences of PF00595 and PF00153, and the right four figures are for the MCMC samples, MC1162 and MC1445 that are obtained in the Boltzmann machine learnings for PF00595 and PF00153, respectively.

TABLE 2
Regularization Parameters and Characteristics of Boltzmann Machines^a with the ModAdam Method for PF00595.

MSA	regularizers	λ_1	λ_2	#Iter ^b	D_1^{KL}	D_2^{KL}	$\delta\psi^2/L$	$(\overline{\psi} - \delta\psi^2)/L$	$\overline{\psi}_N/L$ ^e	$\overline{\psi}_{MC}/L$ ^f	Precision ^g
PF00595	L2-GL1	0.100/ N_{eff}	$= \lambda_1$	1250	0.00506	0.0709	3.23	-3.64	-3.64	-3.29	0.565
PF00595 ^h	L2-GL1	0.100/ N_{eff}	40.0/ N_{eff}	1162 [†]	0.00369	0.0759	2.75	-3.15	-3.15	-2.79	0.588
										(-2.81 ⁱ)	
MC1162 [‡]	L2-GL1	0.100/ N_{eff}	40.0/ N_{eff}	1151	0.00283	0.0689	2.61	-2.98	-2.80	-2.63	0.500
									(-2.82 ^j)		
MC1162 [‡]	L2-GL1	0.891/ N_{eff}	$= \lambda_1$	1280	0.00296	0.0621	2.76	-3.14	-3.15	-2.93	0.457
MC1162 ^{‡h}	L2-GL1	0.891/ N_{eff}	12.6/ N_{eff}	1183	0.00275	0.0646	2.63	-3.00	-3.00	-2.79	0.483
										(-2.93 ^j)	
PF00595	L2-L1 ^k	0.100/ N_{eff}	$= \lambda_1$	1201	0.00674	0.0747	3.19	-3.60	-3.61	-3.31	0.563
PF00595 ^h	L2-L1 ^k	0.100/ N_{eff}	0.316/ N_{eff}	1007	0.00497	0.0736	3.08	-3.48	-3.49	-3.13	0.560
PF00595	L2-L2	0.100/ N_{eff}	$= \lambda_1$	1047	0.00580	0.0737	3.13	-3.54	-3.55	-3.27	0.557
PF00595 ^h	L2-L2	0.100/ N_{eff}	25.1/ N_{eff}	1119	0.00387	0.0725	2.99	-3.39	-3.39	-3.04	0.551

^a Boltzmann machine learning is carried out with more iterations than 1200 by the modified Adam gradient-descent method with $\rho_m = 0.9$, $\rho_v = 0.999$, and an initial learning rate, $\kappa_0 = 0.01$; see methods S.1.8. The number of MCMC samples in the Metropolis-Hastings method is equal to the effective number of sequences; $N_{MC} \approx N_{eff}$.

^b The iteration number corresponding to $\min D_2^{KL}$ over the iteration numbers larger than 1000.

^c The variance per residue of the evolutionary energies of random sequences.

^d $\langle \psi_N(\sigma) \rangle / L$: the ensemble average of evolutionary energy per residue in the Boltzmann distribution by the Gaussian approximation for the distribution of the evolutionary energies of random sequences with the mean $\overline{\psi}$ and the variance $\delta\psi^2$; the Ising gauge is employed.

^e The sample average of evolutionary energies per residue over the sequences with no deletion in the MSA; the Ising gauge is employed.

^f The average of evolutionary energies per residue over the MCMC samples with no deletion; the Ising gauge is employed.

^g Precision of contact prediction; the number of predicted contacts is 352, which is equal to the total number of closely located residue pairs within 8 Å between side-chain centers in the 3D protein structure. The corrected Frobenius norm of couplings is employed for the contact score [10], [11].

^h The optimum set of regularization parameters, which is indicated by bold fonts.

ⁱ The average of evolutionary energies per residue over the MCMC samples with no deletion, 3317 of the total 100000 samples.

^j The sample average of evolutionary energies per residue over the natural proteins with no deletion.

^k The L1 means the elastic net with $\theta_2 = 0.9$ in Eq. S46.

[‡] MCMC samples corresponding to [†].

Here the L2-L2 regularization is employed instead of the L2-GL1 regularization. The same regularization parameters, which have been tuned for the L2-L2 regularization as described in the preceding section, are employed for all gradient-descent methods. Although all the methods attain similar precisions in contact prediction as shown in Table 4, the inferred couplings and the profile of evolutionary energy along the learning process are very different among the gradient-descent methods.

In Fig. 2, the averages of Kullback-Leibler divergences, D_2^{KL} for pairwise marginal distributions and D_1^{KL} for single site marginal distributions, which are defined by Eqs. S70 and S71, are plotted against the iteration number of learning in pink for the ModAdam, in black for the Adam, NAG, and RPROP-LR. The fluctuations of D_2^{KL} and D_1^{KL} at large iteration numbers primarily originate in the statistical error of marginal frequencies estimated by the MCMC sampling. In the ModAdam method, D_2^{KL} converge

TABLE 3
Regularization Parameters and Characteristics of Boltzmann Machines^a with the ModAdam Method for PF00153.

MSA	regularizers	λ_1	λ_2	#Iter ^b	D_1^{KL}	D_2^{KL}	$\delta\psi^2/L$ ^c	$(\bar{\psi} - \delta\psi^2)/L$ ^d	$\overline{\psi}_N/L$ ^e	$\overline{\psi}_{MC}/L$ ^f	Precision ^g
PF00153	L2-GL1	0.100/ N_{eff}	$= \lambda_1$	1084	0.00342	0.0264	2.71	-3.02	-3.29	-3.04	0.596
PF00153^h	L2-GL1	0.100/ N_{eff}	209/ N_{eff}	1445 [†]	0.00112	0.0318	2.50	-2.82	-2.83	-2.54 (-2.51 ⁱ)	0.630
MC1445 [‡]	L2-GL1	0.100/ N_{eff}	209/ N_{eff}	1390	0.00151	0.0323	2.48	-2.82	-2.54 (-2.83 ^j)	-2.52	0.630
MC1445 [‡]	L2-GL1	7.94/ N_{eff}	$= \lambda_1$	1181	0.000975	0.0160	2.25	-2.57	-2.57	-2.47	0.551
MC1445^{‡h}	L2-GL1	7.94/ N_{eff}	20.0/ N_{eff}	1197	0.000985	0.0162	2.24	-2.55	-2.55	-2.43 (-2.64 ^j)	0.557
PF00153	L2-L1 ^k	0.100/ N_{eff}	$= \lambda_1$	1149	0.00313	0.0265	2.73	-3.05	-3.32	-3.09	0.599
PF00153^h	L2-L1 ^k	0.100/ N_{eff}	25.1/ N_{eff}	1208	0.00165	0.0318	2.57	-2.91	-2.91	-2.66	0.557
PF00153	L2-L2	0.100/ N_{eff}	$= \lambda_1$	1223	0.00329	0.0264	2.76	-3.08	-3.35	-3.10	0.605
PF00153^h	L2-L2	0.100/ N_{eff}	398/ N_{eff}	1066	0.00119	0.0336	2.55	-2.87	-2.86	-2.52	0.569

^a Boltzmann machine learning is carried out with more iterations than 1200 by the modified Adam gradient-descent method with $\rho_m = 0.9$, $\rho_v = 0.999$, and an initial learning rate, $\kappa_0 = 0.01$; see methods S.1.8. The number of MCMC samples in the Metropolis-Hastings method is equal to the effective number of sequences; $N_{MC} \approx N_{\text{eff}}$.

^b The iteration number corresponding to $\min D_2^{KL}$ over the iteration numbers larger than 1000.

^c The variance per residue of the evolutionary energies of random sequences

^d $\langle \psi_N(\sigma) \rangle / L$; the ensemble average of evolutionary energy per residue in the Boltzmann distribution by the Gaussian approximation for the distribution of the evolutionary energies of random sequences with the mean $\bar{\psi}$ and the variance $\delta\psi^2$; the Ising gauge is employed.

^e The sample average of evolutionary energies per residue over the sequences with no more than 2 deletions for PF00153 and with no more than 3 for the MCMC samples; the Ising gauge is employed.

^f The average of evolutionary energies per residue over the MCMC samples with no more than 3 deletions; the Ising gauge is employed.

^g Precision of contact prediction; the number of predicted contacts is 332, which is equal to the total number of closely located residue pairs within 8 Å between side-chain centers in the 3D protein structure. The corrected Frobenius norm of couplings is employed for the contact score [10], [11].

^h The optimum set of regularization parameters, which is indicated by bold fonts.

ⁱ The average of evolutionary energies per residue over the MCMC samples with no deletion, 207 of the total 100000 samples.

^j The sample average of evolutionary energies per residue over the natural proteins with no more than 2 deletions.

^k The L1 means the elastic net with $\theta_2 = 0.9$ in Eq. S46.

[†] MCMC samples corresponding to [†].

TABLE 4
Comparison of the Learning Methods^a for Gradient Descent on PF00595.

Learning method	regularizers	λ_1	λ_2	#Iter ^b	D_1^{KL}	D_2^{KL}	$\delta\psi^2/L$ ^c	$(\bar{\psi} - \delta\psi^2)/L$ ^d	$\overline{\psi}_N/L$ ^e	$\overline{\psi}_{MC}/L$ ^f	Precision ^g
ModAdam ^h	L2-L2	0.100/ N_{eff}	25.1/ N_{eff}	1119	0.00387	0.0725	2.99	-3.39	-3.39	-3.04	0.551
(second run) ⁱ				2018	0.00372	0.0696	3.12	-3.53	-3.52	-3.16	0.568
Adam ^h	L2-L2	0.100/ N_{eff}	25.1/ N_{eff}	1012	0.00320	0.0681	3.35	-3.73	-3.59	-3.23	0.563
NAG ^h	L2-L2	0.100/ N_{eff}	25.1/ N_{eff}	1110	0.00381	0.0724	2.94	-3.34	-3.34	-3.01	0.557
				2095	0.00361	0.0690	3.08	-3.48	-3.48	-3.12	0.565
RPROP-LR ^j	L2-L2	0.100/ N_{eff}	25.1/ N_{eff}	1052	0.00391	0.0766	2.97	-3.36	-3.28	-2.95	0.560

^a Boltzmann machine learning is carried out with more iterations than 1200 by each gradient-descent method; see methods S.1.8. The number of MCMC samples in the Metropolis-Hastings method is equal to the effective number of sequences; $N_{MC} \approx N_{\text{eff}}$.

^b The iteration number corresponding to $\min D_2^{KL}$ over the iteration numbers larger than 1000.

^c The variance per residue of evolutionary energies of random sequences

^d $\langle \psi_N(\sigma) \rangle / L$; the ensemble average of evolutionary energy per residue in the Boltzmann distribution by the Gaussian approximation for the distribution of the evolutionary energies of random sequences with the mean $\bar{\psi}$ and the variance $\delta\psi^2$; the Ising gauge is employed.

^e The average of evolutionary energies per residue over the homologous sequences with no deletion in the MSA; the Ising gauge is employed.

^f The average of evolutionary energies per residue over the MCMC samples with no deletion; the Ising gauge is employed.

^g Precision of contact prediction; the number of predicted contacts is 352, which is equal to the total number of closely located residue pairs within 8 Å between side-chain centers in the 3D protein structure. The corrected Frobenius norm of couplings is employed for the contact score [10], [11].

^h The initial learning rates and other hyper-parameters are ($\kappa_0 = 0.01, \rho_m = 0.9, \rho_v = 0.999$) for the ModAdam, ($\kappa_0 = 0.001, \rho_m = 0.9, \rho_v = 0.999$) for the Adam, and ($\kappa_0 = 0.1, \rho_m = 0.95$) for the NAG; see methods S.1.8.

ⁱ The iteration number corresponding to $\min D_2^{KL}$ over the iteration numbers larger than 2000; more than 2100 iterations are carried out.

^j The RPROP learning rate method [12]; the learning rates are limited between 10^{-5} and 10.

more slowly and its fluctuations seem to be larger than in the other methods. However, a more important thing is the reasonable inference of fields and couplings.

Let us see how the single-site frequencies and pairwise correlations are recovered in each method, and how the inferred fields and couplings differ among the gradient-descent methods. The fields and couplings as well as the marginal single-site frequencies and pairwise correlations are compared between the ModAdam and Adam methods in Fig. 3 and Fig. S1. It should

be noticed here that fields and couplings are expressed in the Ising gauge for comparison. Although the single-site marginal probabilities in both models almost coincide with each other, there are some fields that are significantly more positive in the Adam than in the ModAdam. On the other hand, strong couplings are significantly underestimated by the Adam in the comparison with the ModAdam. Consistently, the pairwise correlations are slightly under-reproduced in the region of strong correlations. As a result, the negative correlation between couplings and residue-

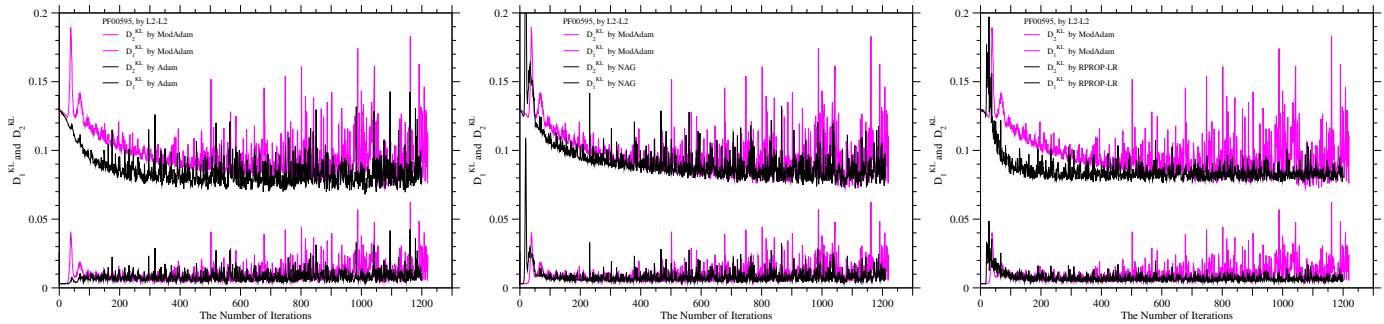


Fig. 2. Learning processes by the ModAdam, Adam, NAG, and RPROP-LR gradient-descent methods for PF00595. The averages of Kullback-Leibler divergences, D_{KL}^2 for pairwise marginal distributions and D_{KL}^1 for single-site marginal distributions, are drawn against iteration number in the learning processes. D_{KL}^2 and D_{KL}^1 for the Adam, NAG, and RPROP-LR are indicated by the upper and lower black lines in the left, middle, and right figures, respectively, and those for the ModAdam are shown in pink in all figures for comparison. The L2-L2 regularization model is employed. The values of hyper-parameters are listed in Table 4 as well as others.

residue distance is better detected by the ModAdam than by the Adam method as shown in Fig. 4, in which $J_{ij}(a_k, a_l)$, where $(a_k, a_l) = \operatorname{argmax}_{a_k, a_l \neq \text{deletion}} |J_{ij}(a_k, a_l)|$ in the Ising gauge, are plotted against the distance between i th and j th residues; all residue pairs with $|J_{ij}(a_k, a_l)| \geq 0.73$ in either method are in contact within 8 Å, but there are only 6 such pairs in the Adam but 16 pairs in the ModAdam; only amino acid pairs are taken into account in the argmax, because deletions within gaps in Pfam alignments tend to have large positive correlations. This tendency is very clear even at the small number of iterations; see Fig. S2. Even if gradient-descent methods attain to a similar solution via different intermediate states, it will be desirable to attain with a limited number of iterations to approximate solutions that satisfy characteristics required for the solution. Here it is noteworthy that the fields and couplings inferred by the NAG almost coincide with those by the ModAdam; see Fig. 3 and Fig. S3. Hence, these results indicate that the stepsize of parameter updates must be proportional to the partial derivative in order to correctly estimate the dependencies of couplings J_{ij} on the distance between residues i and j . The parameters inferred by the Adam likely include as much information of contact ranks as those by the ModAdam, because as shown in Table 4 the precision of contact prediction by the Adam is as good as that by the ModAdam. It should be noticed, however, that the present purpose is to correctly infer not only the ranks but also couplings and fields. In the Adam method, a stepsize for each parameter update is proportional to the partial derivative that is normalized for each parameter at each step, so that stepsizes are essentially in the same order for all parameters at each iteration, making the Adam suitable to similarly dense interaction systems as well as the L_2 regularization.

RPROP, in which the stepsize does not depend on the value of the partial derivative but on its sign, was modified [12] for inverse Potts problems to be proportional to the partial derivative. This modified RPROP is called here RPROP-LR. In Fig. 3 and Fig. S4, the fields and couplings inferred by the RPROP-LR method are shown in comparison with those by the ModAdam as well as the marginal single-site probabilities and pairwise correlations. The RPROP-LR method is, like Adam, a per-parameter adaptive learning rate method but unlike Adam it does not normalize each partial derivative of parameter. As a result, the RPROP-LR infers couplings similarly to the ModAdam. From these figures, it is hard to judge which is better, ModAdam or RPROP-LR. However, the sample and ensemble averages of evolutionary energy along the

learning process provide more useful information with respect to the characteristics of each gradient-descent method.

In Fig. 5, the average evolutionary energy per residue ($\overline{\psi_N}/L$) of natural sequences and the ensemble average of evolutionary energy per residue ($(\overline{\psi} - \delta\psi^2)/L$) are plotted against the iteration number for each method. These profiles are well reproducible by another run of Boltzmann machine learning. In the figure for the ModAdam method, both the results of the first and second runs are shown by dots and solid lines, respectively. They indistinguishably overlap to each other. The profile of evolutionary energy along the learning process is very different among the gradient-descent methods. The average of evolutionary energies over natural proteins, $\overline{\psi_N}$, as well as D_2^{KL} more quickly converges in the RPROP-LR and Adam than in the ModAdam. However, a more important feature is that the sample average of evolutionary energies over natural sequences, $\overline{\psi_N(\sigma_N)}$, is higher than $(\overline{\psi} - \delta\psi^2)$ with the interaction parameters inferred by the Adam and RPROP-LR methods under the regularization parameters under which they are equal to each other in the ModAdam method. It should be recalled that $(\overline{\psi} - \delta\psi^2)/L$ approximates the ensemble average $\langle \psi_N(\sigma) \rangle_\sigma$ of evolutionary energy in the Boltzmann distribution; see Eq. S9. The fact that $\overline{\psi_N(\sigma_N)} > (\overline{\psi} - \delta\psi^2)$ indicates that the fields and couplings inferred by the Adam and the RPROP-LR are less favorable to the natural proteins than those by the ModAdam under the same condition. In other words, the ModAdam method is better to infer more reasonable interaction parameters for protein sequences than the Adam and the RPROP-LR. In addition, D_2^{KL} of the MCMC samples obtained by the RPROP-LR is higher than that of the ModAdam as shown in Table 4, indicating that the recoverability of pairwise frequencies is less in the RPROP-LR than in the ModAdam.

The NAG method is not a per-parameter learning rate method and employs a stepsize that is proportional to the partial derivative in common with the ModAdam. As a result, the fields and couplings inferred by the NAG almost coincide with those by the ModAdam. However, the sample and ensemble averages of evolutionary energy converge a little higher values in the NAG than in the ModAdam, indicating that the fields and couplings are slightly more optimized by the ModAdam.

The Adam method as well as L_2 regularization is not appropriate to the present Potts problem, because residue-residue interactions in proteins are very sparse. On the other hand, the RPROP-LR appears to be inferior to the ModAdam and NAG with

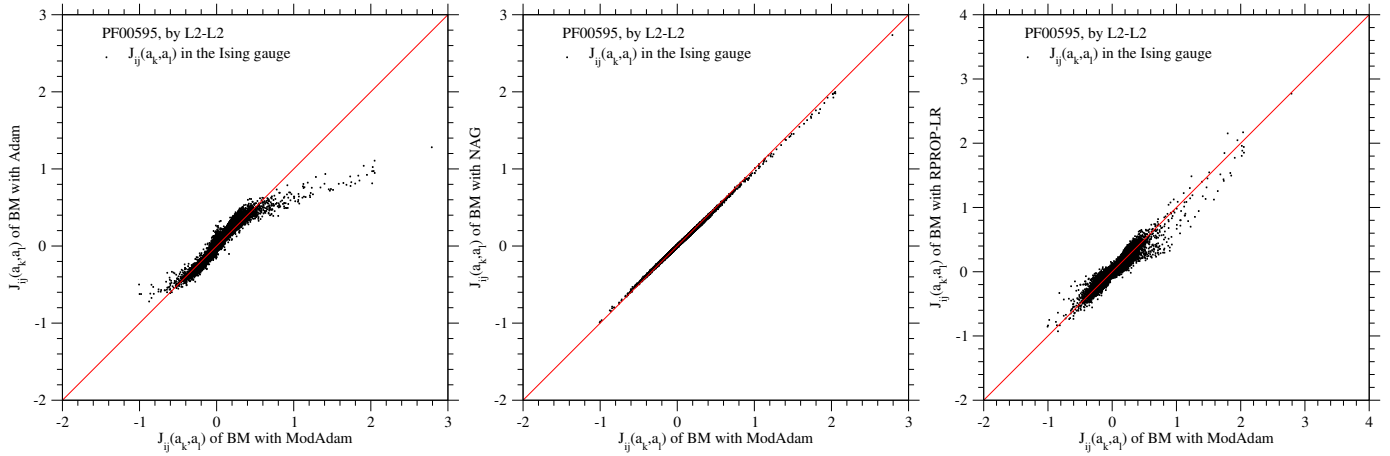


Fig. 3. Comparisons of the inferred couplings $J_{ij}(a_k, a_l)$ in the Ising gauge between the ModAdam and the other gradient-descent methods, Adam, NAG, and RPROP-LR, for PF00595. The abscissas correspond to the couplings inferred by the modified Adam, and the ordinates correspond to those by the Adam, NAG, and RPROP-LR in order from the left to the right. The regularization model L2-L2 is employed for all methods. The solid lines show the equal values between the ordinate and abscissa. The values of hyper-parameters are listed in Table 2. The overlapped points of $J_{ij}(a_k, a_l)$ in the units 0.001 are removed.

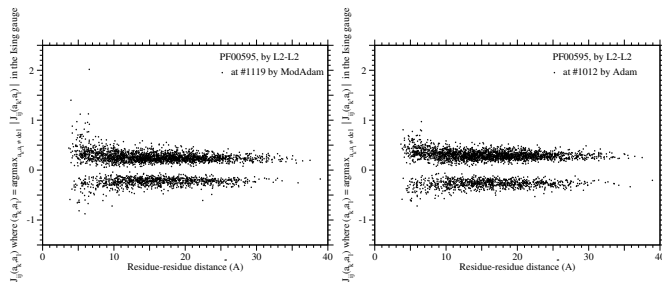


Fig. 4. Differences in the learning of coupling parameters, $J_{ij}(a_k, a_l)$, between the ModAdam and Adam gradient-descent methods for PF00595. All $J_{ij}(a_k, a_l)$ where $(a_k, a_l) = \operatorname{argmax}_{a_k, a_l \neq \text{deletion}} |J_{ij}(a_k, a_l)|$ in the Ising gauge are plotted against the distance between i th and j th residues. The ModAdam and Adam methods are employed for the left and right figures, respectively. The regularization model L2-L2 is employed for both methods. The learning processes by both methods are shown in Fig. 2. Please notice that more strong couplings tend to be inferred for closely located residue pairs by the ModAdam method than by the Adam method. The values of hyper-parameters are listed in Table 2.

respect to the quality of inferred interactions, although it quickly converges and infers couplings similar to those by ModAdam. Thus, the ModAdam method is employed in the following; see methods S.1.8.

2.4 Dependences of Inferred Parameters on the Regularization Models: the Effects of the Group L_1 Regularization

The profiles of the average evolutionary energies of PF00595 and PF00153 in the learning processes with the L2-GL1 regularization are shown in Fig. 6; the values of the regularization parameters are listed in Tables 2 and 3. It is clear that both $\overline{\psi}_N$ and $\overline{\psi} - \delta\psi^2$ almost converge. In Fig. 7 and Fig. S5, the $J_{ij}(a_k, a_l)$, where $(a_k, a_l) = \operatorname{argmax}_{a_k, a_l \neq \text{deletion}} |J_{ij}(a_k, a_l)|$ in the Ising gauge, are plotted against the distance between i th and j th residues for each regularization model. The negative correlation of coupling interactions on residue-residue distance is clearly shown in all models. On the other hand, there is not an energy gap at the value zero for $J_{ij}(a_k, a_l)$ in the L2-GL1 but in the other models, indicating that the group- L_1 regularization is effective to yield

sparsity in the couplings. It should be noticed here that in the present work the L_1 for couplings means the elastic net including a small contribution of L_2 in addition to the L_1 regularization to avoid non-unique solutions; see Eq. S46.

The direct comparisons of the inferred fields and couplings between the L2-GL1 and the other regularization models are shown in Fig. 8 for PF00595 and Fig. 9 for PF00153; also see Figs. S6 and S7 for marginal single-site probabilities and pairwise correlations. There is no significant difference in the inferred fields between the regularization models. On the other hand, weak couplings are differently inferred between the L2-GL1 and the other models, and the differences of their estimates clearly show the typical characteristics of the group- L_1 model that the coupling interactions are estimated sparsely in the L2-GL1 model. Coupling interactions except for nearly non-interacting residue pairs are inferred to be weaker in the L2-L2 than L2-GL1, but in the L2-L1 similarly to the L2-GL1. This tendency is more clearly shown for PF00153 consisting of more sequences than for PF00595.

In Fig. 10, the precisions of contact prediction based on contact score, which is defined as the corrected Frobenius norm of couplings [10], [11], are compared among the regularization models; residues whose side chain centers are within 8 Å in a three-dimensional protein structure are defined here to be in contact, including neighboring residue pairs along a sequence. The L2-GL1 model performs better in a whole range of contact ranks than the L2-L1 and L2-L2 models. Consistently, the better performance of the L2-GL1 model is more clear for PF00153 that consists of more effective sequences than PF00595. The better performance of the L2-GL1 than the others is, however, less than 0.04 in precision for PF00595 and 0.08 for PF00153.

2.5 Recoverabilities of Single-Site Frequencies and Pairwise Correlations in the L2-GL1 Regularization Model

Recoverabilities of single-site frequencies and pairwise correlations in the L2-GL1 model are shown in Fig. 11 and in Figs. S9 and S10, and are also indicated by the values of D_1^{KL} and D_2^{KL} listed in Tables 2 and 3. Although single-site and pairwise amino acid probabilities are well recovered in both protein families, they are better recovered as expected in PF00153 consisting

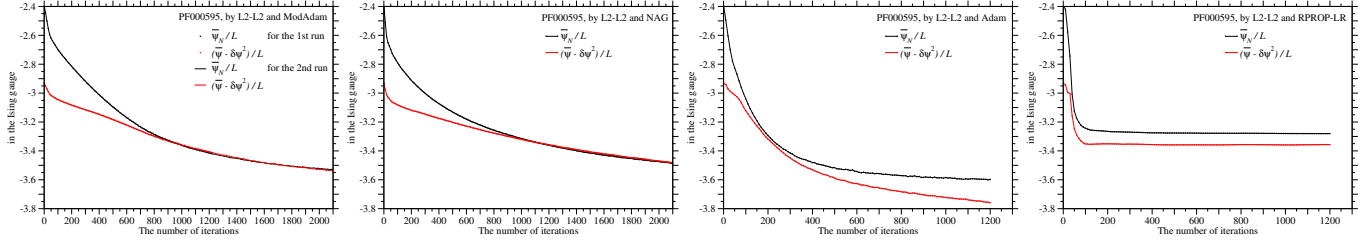


Fig. 5. The profile of the average evolutionary energies along the learning process in the L2-L2 model by each gradient-descent method for PF00595. The average evolutionary energy per residue $\overline{\psi}_N/L$ of natural sequences and the ensemble average of evolutionary energy per residue in the Gaussian approximation $(\overline{\psi} - \delta\psi^2)/L$ in the Ising gauge are plotted every 10 iterations against iteration number in the learning by each of the ModAdam, NAG, Adam, and RPROP-LR in the order of the left to the right; the sample and ensemble averages are indicated by the upper and lower lines, respectively. The L2-L2 regularization model is employed. For the ModAdam in the leftmost figure, those for the first run of 1220 iterations and for the second run, which is conditioned to run by more than 2000 iterations, are plotted by dots and solid lines, respectively; they indistinguishably overlap.

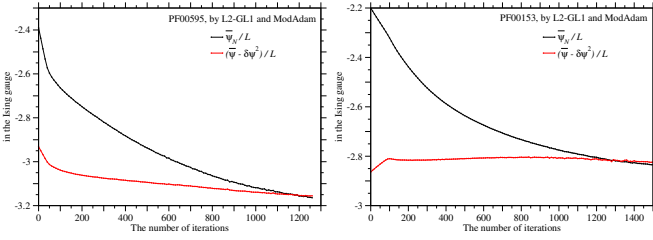


Fig. 6. The profiles of the average evolutionary energies along the learning process in the L2-GL1 model by the ModAdam for PF00595 and PF00153. The average evolutionary energy per residue $\overline{\psi}_N/L$ of natural sequences and the ensemble average of evolutionary energy per residue in the Gaussian approximation $(\overline{\psi} - \delta\psi^2)/L$ in the Ising gauge are plotted every 10 iterations against iteration number in the learning by the ModAdam; the sample and ensemble averages are indicated by the upper and lower lines, respectively. The left and right figures are for PF00595 and PF00153, respectively. The L2-GL1 regularization model is employed. The values of the regularization parameters are listed in Tables 2 and 3.

of more effective number of sequences than PF00595; Both $D_1^{KL} = 0.00112$ and $D_2^{KL} = 0.0318$ for PF00153 are less than half of $D_1^{KL} = 0.00369$ and $D_2^{KL} = 0.0759$ for PF00595, even though λ_2 is larger for PF00153 than PF00595. It should be noticed, however, that the correlations, $C_{ij}(a_k, a_l) \equiv P_{ij}(a_k, a_l) - P_i(a_k)P_j(a_l)$, are under-reproduced with this set of the regularization parameters for strongly correlated site pairs in both proteins.

2.6 Reproducibilities of Fields and Couplings in the L2-GL1 Model

Now let us consider how well the Boltzmann machine can infer fields and couplings from protein sequence data. Reproducibilities of fields and couplings have been examined for artificial interactions on a lattice protein and others [12]. Here, MCMC samples that are generated with the fields and couplings inferred by the Boltzmann machine for the protein families are employed as protein-like sequences for which the Boltzmann machine learning with the same regularization model and gradient-descent method is executed again in order to examine how well the Boltzmann machine can reproduce the fields and couplings in protein-like sequences.

MC1162 listed in Table 2 and MC1445 in Table 3 are MCMC samples generated with the fields and couplings inferred for PF00595 and for PF00153, respectively. First, the regularization parameters optimized in the first stage have been employed for the Boltzmann machine in the second stage. Ideally, the condition, $(\overline{\psi} - \delta\psi^2) \sim \overline{\psi}_N$, should be satisfied with this set

of regularization parameters. In the interactions inferred in the first stage, however, the average evolutionary energies of MCMC samples are higher than those of the natural protein families. As a result, $\langle \psi_N(\sigma) \rangle_\sigma < \overline{\psi}_N$ is obtained with the same regularization parameters in the second stage,

The sample averages of the following evolutionary energies take similar values in both set of interactions inferred in the first and second stages except $\overline{\psi}_{PF00595}$; $\overline{\psi}_{PF00595} = -3.15 < -2.82$, $\overline{\psi}_{MC1162} = -2.79 \sim -2.80$, $\overline{\psi}_{PF00153} = -2.83 \sim -2.83$, and $\overline{\psi}_{MC1445} = -2.54 \sim -2.54$ in the interactions inferred in the first and second stages, respectively, and $\langle \psi_N(\sigma) \rangle_\sigma \sim \overline{\psi}_{PF00595} \leq \overline{\psi}_{MC1162}$ and $\langle \psi_N(\sigma) \rangle_\sigma \sim \overline{\psi}_{PF00153} \leq \overline{\psi}_{MC1445}$ are satisfied in both the interactions. This fact indicates that the interactions inferred in the second stage also favor the natural protein families, and in this aspect those inferred in the first stage are well recovered in the second stages, although the optimum condition, $\langle \psi_N(\sigma) \rangle_\sigma \sim \overline{\psi}_N$, is not satisfied. However, let us tune the regularization parameters without a priori knowledge according to the procedure described in the preceding section. Regularization parameters optimized in the second stage are listed in Table 2 and 3.

The single-site frequencies and pairwise correlations recovered in the second stage are compared with those in the first stage and also with the natural proteins in Fig. 12 and in Figs. S11 and S12. The single-site frequencies and pairwise correlations are extremely well recovered in the second stage for PF00153 consisting of more sequences than PF00595. Pairwise correlations are slightly under-reproduced for strongly correlated site pairs of PF00595 as well as in the first stage. The smaller values of λ_2 in the second stage than in the first stage cause single-site frequencies and pairwise correlations to be better recovered and also smaller D_1^{KL} and D_2^{KL} in the second stage than in the first stage.

In Figs. 13 and 14, the fields and couplings inferred in the second stage are compared with true ones, that is, those inferred in the first stage. Both are well recovered, although strong couplings are always underestimated in both proteins. Large errors may be included in the estimates for weak couplings of $|J_{ij}(a_k, a_l)| < -0.6$. Noise being included in the couplings is expected to increase as λ_2 decreases in the second stage.

2.7 Reproducibility of the Evolutionary Energy Distribution of Natural Proteins by MCMC Samples in the L2-GL1 Model

It has been shown [14] that pairwise coevolutionary models capture the collective residue variability across homologous proteins even for quantities which are not imposed by the inference proce-

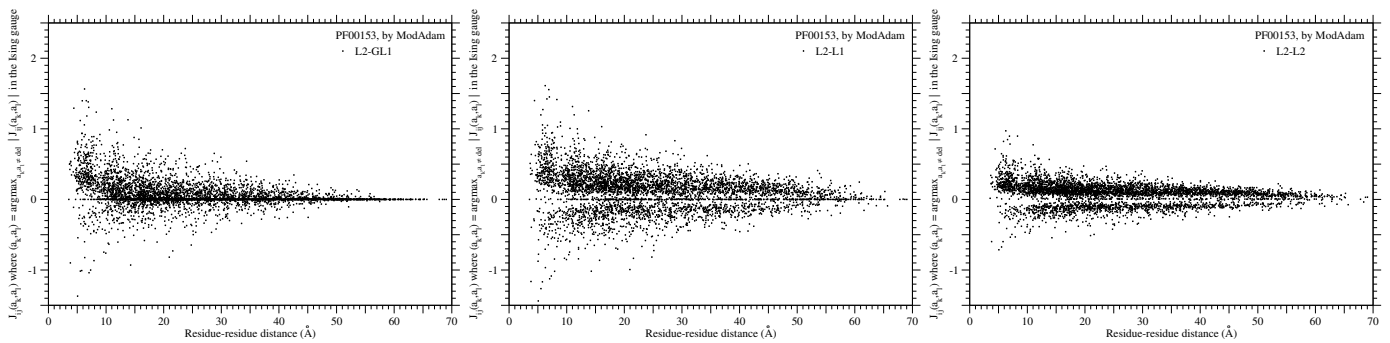


Fig. 7. Differences of inferred couplings $J_{ij}(a_k, a_l)$ among the regularization models for PF00153. All $J_{ij}(a_k, a_l)$ where $(a_k, a_l) = \text{argmax}_{a_k, a_l \neq \text{deletion}} |J_{ij}(a_k, a_l)|$ in the Ising gauge are plotted against the distance between i th and j th residues. The regularization models L2-GL1, L2-L1, and L2-L2 are employed for the left, middle, and right figures, respectively. The protein family PF00153 is employed. The values of regularization parameters are listed in Table 3.

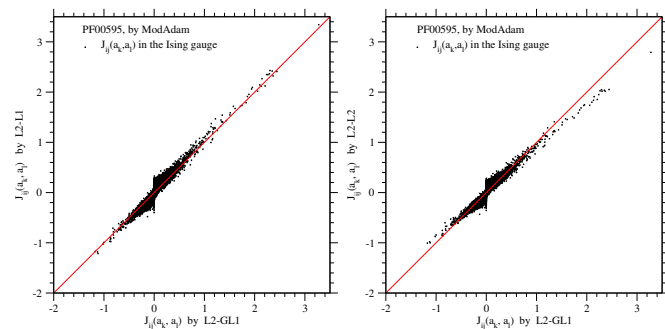


Fig. 8. Comparisons of inferred couplings $J_{ij}(a_k, a_l)$ in the Ising gauge between the regularization models for PF00595. Both abscissa correspond to the couplings inferred by the L2-GL1. The ordinates in the left and right figures correspond to the couplings inferred by the L2-L1 and L2-L2 models, respectively. The values of regularization parameters are listed in Table 2. The solid lines show the equal values between the ordinate and abscissa. The overlapped points of $J_{ij}(a_k, a_l)$ in the units 0.001 are removed.

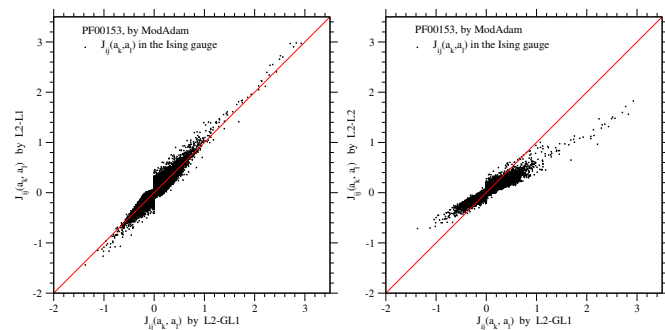


Fig. 9. Comparisons of inferred couplings $J_{ij}(a_k, a_l)$ in the Ising gauge between the regularization models for PF00153. Both abscissa correspond to the couplings inferred by the L2-GL1. The ordinates in the left and right figures correspond to the couplings inferred by the L2-L1 and L2-L2 models, respectively. The values of regularization parameters are listed in Table 3. The solid lines show the equal values between the ordinate and abscissa. The overlapped points of $J_{ij}(a_k, a_l)$ in the units 0.001 are removed.

ture, like three-residue correlations and the sequence distances between homologs. However, as listed in Tables 2 and 3 the average evolutionary energies of natural proteins in PF00595 and in PF00153 are significantly lower than those of MCMC samples obtained by the Boltzmann machine learnings. The same fact was also reported for the Pfam family PF00014 [12]. In Fig. 15, the

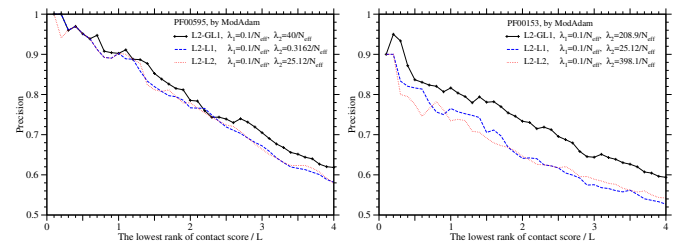


Fig. 10. Precision of each regularization model in the contact predictions for PF00595 and PF00153. Precisions of contact predictions are compared between the regularization models. The ordinate of each figure corresponds to the precision of contact prediction, in which residue pairs are predicted as contacts in the decreasing order of contact score, and the number of predicted contacts is indicated as (the lowest rank of contact score) $/L$ by the abscissa. Residues whose side chain centers are within 8 Å in the 3D protein structure are defined to be in contact; neighboring residue pairs along the sequence are included. The left and right figures are for the protein families PF00595 and PF00153, respectively. The solid, broken, and dotted lines correspond to the regularization models, L2-GL1, L2-L1, and L2-L2, respectively. The corrected Frobenius norm of couplings is employed for the contact score [10], [11].

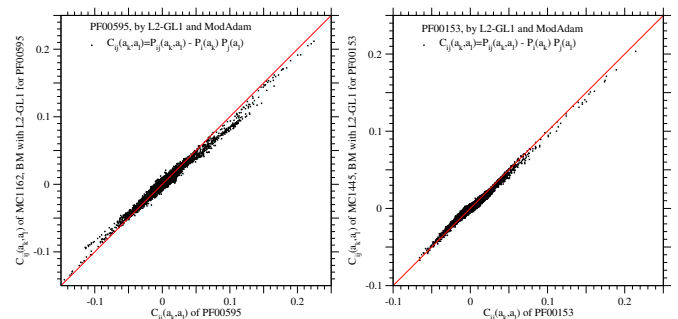


Fig. 11. Recoverabilities of the pairwise correlations of PF00595 and PF00153 by the Boltzmann machine learning with the L2-GL1 model and the ModAdam method. The left and right figures are for PF00595 and PF00153, respectively; $D_2^{KL} = 0.0759$ for PF00595 and $D_2^{KL} = 0.0318$ for PF00153. The solid lines show the equal values between the ordinate and abscissa. The overlapped points of $C_{ij}(a_k, a_l)$ in the units 0.0001 are removed. See Tables 2 and 3 for the regularization parameters employed.

histograms of evolutionary energies are compared with between the natural protein families, PF00595 and PF00153, and the MCMC samples obtained by the Boltzmann machine learnings. Here, only sequences with no deletion for PF00595 and with a few deletions for PF00153 are employed. It is clear that the

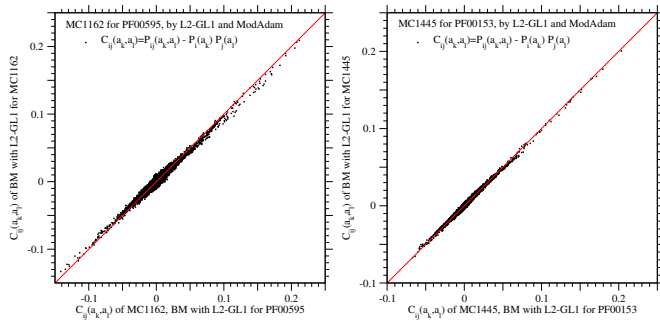


Fig. 12. Recoverabilities of the pairwise correlations by the Boltzmann machine learning with the L2-GL1 model and the ModAdam method for the protein-like sequences, the MCMC samples that are obtained by the same Boltzmann machine for PF00595 and PF00153. The MCMC samples obtained by the Boltzmann machine learning with the L2-GL1 model and the ModAdam method for PF00595 and PF00153 are employed as protein-like sequences for which the Boltzmann machine learning with the same model and method is executed again in order to examine how precisely the marginals of protein-like sequences can be recovered. The marginals recovered by the Boltzmann machine learning for the MCMC samples are compared to those of the MCMC samples. The left and right figures are for the single-site probabilities and pairwise correlations, respectively. The solid lines show the equal values between the ordinate and abscissa. The overlapped points of $C_{ij}(a_k, a_l)$ in the units 0.0001 are removed. See Tables 2 and 3 for the regularization parameters employed.

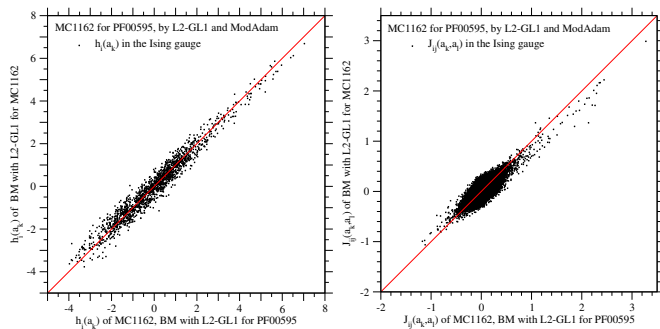


Fig. 13. Reproducibility of the fields and couplings in the Ising gauge by the Boltzmann machine learning with the L2-GL1 model and the ModAdam method for the protein-like sequences, the MCMC samples that are obtained by the same Boltzmann machine for PF00595. The MCMC samples obtained by the Boltzmann machine learning with the L2-GL1 model and the ModAdam method for PF00595 are employed as protein-like sequences for which the Boltzmann machine learning with the same model and method is executed again in order to examine how well the fields and couplings in the protein-like sequences can be reproduced. The fields and couplings inferred by the Boltzmann machine learning for the MCMC samples are plotted against the actual values of their interactions in the left and right figures, respectively. The solid lines show the equal values between the ordinate and abscissa. The overlapped points of $J_{ij}(a_k, a_l)$ in the units 0.001 are removed. See Table 2 for the regularization parameters employed.

MCMC samples cannot well reproduce the natural proteins with respect to the evolutionary energy distribution. This discrepancy of the energy distributions may indicate the insufficient equilibration owing to frustrated interactions. It is not improved, however, even by increasing the number of MCMC samples from $N_{MC} = N_{eff}$ to 100000. Also, it should be noticed that the discrepancy of the average evolutionary energy between the target sequences and the MCMC samples is improved when the MCMC samples rather than the natural proteins are used as protein-like sequences; see Tables 2 and 3 and Fig. 15. Thus, recovering the pairwise amino acid frequencies in the resolution of a total energy may be harder for natural proteins than for protein-like sequences.

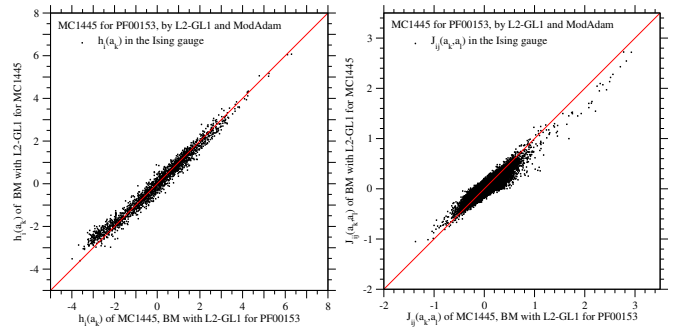


Fig. 14. Reproducibility of the fields and couplings in the Ising gauge by the Boltzmann machine learning with the L2-GL1 model and the ModAdam method for the protein-like sequences, the MCMC samples that are obtained by the same Boltzmann machine for PF00153. The MCMC samples obtained by the Boltzmann machine learning with the L2-GL1 model and the ModAdam method for PF00153 are employed as protein-like sequences for which the Boltzmann machine learning with the same model and method is executed again in order to examine how well the fields and couplings in the protein-like sequences can be reproduced. The fields and couplings inferred by the Boltzmann machine learning for the MCMC samples are plotted against the actual values of their interactions in the left and right figures, respectively. The solid lines show the equal values between the ordinate and abscissa. The overlapped points of $J_{ij}(a_k, a_l)$ in the units 0.001 are removed. See Table 3 for the regularization parameters employed.

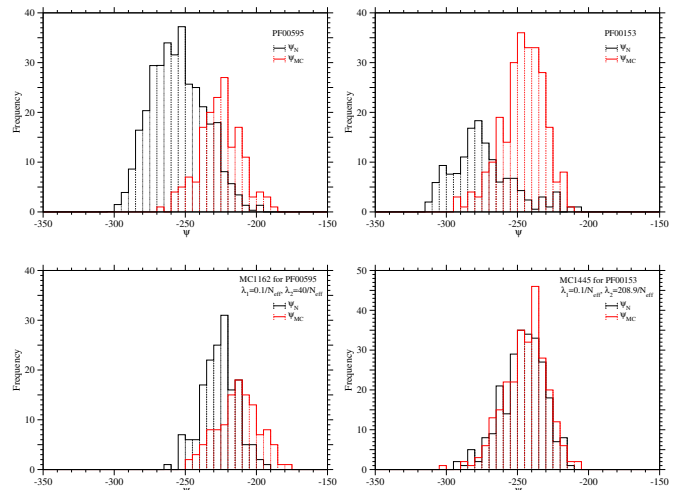


Fig. 15. Comparisons of the histograms of inferred evolutionary energies in the Ising gauge between the target sequences (ψ_N) and the MCMC samples (ψ_{MC}) obtained by the Boltzmann machine learnings. In the upper left and right figures, the evolutionary energies (ψ_N) of the natural proteins are compared with those (ψ_{MC}) of the MCMC samples obtained by the Boltzmann machine learnings for PF00595 and PF00153, respectively. Sequences with no deletion for PF00595 and with no more than 2 deletions for PF00153 are employed; the effective numbers M_{eff} of sequences are 340.0 for PF00595, 139.8 for PF00153. The 162 samples with no deletion in MC1162 and 254 samples with no more than 3 deletions in MC1445 are employed. In the lower left and right figures, the evolutionary energies (ψ_N) of the protein-like sequences, MC1162 and of MC1445, are compared with those (ψ_{MC}) of the MCMC samples obtained by the Boltzmann machine learnings for them. The same regularization parameters as for the natural protein families are employed; $\lambda_2 = 40.0/N_{eff}$ for PF00595 and $\lambda_2 = 209/N_{eff}$ for PF00153, and $\lambda_1 = 0.100/N_{eff}$ for both. The 118 samples with no deletion in the MCMC samples for MC1162 and 268 samples with no more than 3 in the MCMC samples for MC1445 are employed.

2.8 Selective Temperature, T_s

Selective temperature T_s that is defined by Eq. S12, which quantifies how strong the folding/structural constraints are in the evolution of a protein family, has been estimated by vari-

TABLE 5
Selective Temperatures (T_s) Estimated from the Fields and Couplings Inferred for PF00595 and PF00153.

Pfam ID	$\overline{\psi_N}/L$	$\overline{\Delta\psi_N}$	$\overline{Sd(\Delta\psi_N)}$	$\overline{Sd(Sd(\Delta\psi_N))}$	$r_{\psi_N}^d$	$\alpha_{\psi_N}^d$	$r_{\psi_N}^e$	$\alpha_{\psi_N}^e$	r^f	slope ^f	\hat{T}_s	$T_m^{\text{exp } g}$	\hat{T}_g^h	$\hat{\omega}^i$
					for $\overline{\Delta\psi_N}$		for $\overline{Sd(\Delta\psi_N)}$			(kcal/mol)	(°K)	(°K)	(°K)	(k_B)
PF00595	-3.15	3.94	2.64	0.113	-0.980	-1.90	-0.237	-0.113	0.920	0.400	201	313 ^k	215	1.20
PF00153	-2.84	3.36	2.71	0.141	-0.981	-1.91	-0.537	-0.338			196			

^a The average of evolutionary energies per residue over representatives of homologous sequences; the Ising gauge is employed. The representatives of unique sequences with no deletions for PF00595 and with no more than 2 deletions for PF00153, which are at least 20% different from each other, are used; their numbers are 361 for PF00595 and 144 for PF00153.
^b The averages of $\overline{\Delta\psi_N}$ and $\overline{Sd(\Delta\psi_N)}$, which are the mean and the standard deviation of $\Delta\psi_N$ due to single nucleotide nonsynonymous substitutions in a sequence, over the representatives of homologous sequences.
^c The standard deviation of $\overline{Sd(\Delta\psi_N)}$ over the representatives of homologous sequences.
^d The correlation (r_{ψ_N}) and regression coefficients (α_{ψ_N}) of $\Delta\psi_N$ on ψ_N/L ; $\Delta\psi_N \sim \alpha_{\psi_N}\psi_N/L + \beta_{\psi_N}$.
^e The correlation (r_{ψ_N}) and regression coefficients (α_{ψ_N}) of $\overline{Sd(\Delta\psi_N)}$ on ψ_N/L ; $\overline{Sd(\Delta\psi_N)} \sim \alpha_{\psi_N}\psi_N/L + \beta_{\psi_N}$.
^f The reflective correlation (r) and regression coefficient (slope) of the experimental values [65] of folding free energy changes ($\Delta\Delta G_{ND}$) due to single amino acid substitutions on $\Delta\psi_N$ ($\approx \Delta\Delta\psi_{ND}$) for the same types of substitutions; the slope is equal to $k_B T_s$.
^g An experimental value of melting temperature; T_m^{exp} for PF00595 is taken from [66].
^h Glass transition temperature; $(T_s/(2T_m))(1 + (T_m^2/T_g^2)) = 1$. Folding free energy, $\langle \Delta G_{ND}(\sigma, T) \rangle_\sigma = k_B T_s \delta\psi^2 [(T_s/(2T))(1 + (T^2/T_g^2)) - 1]$, is inferred to be -1.4 kcal/mol at $T = 298^\circ\text{K}$ for PF00595, while its experimental value is equal to -2.9 ± 0.2 kcal/mol [67].
ⁱ Conformational entropy per residue; $\omega = (T_s/T_g)^2 \delta\psi^2 / (2L)$.

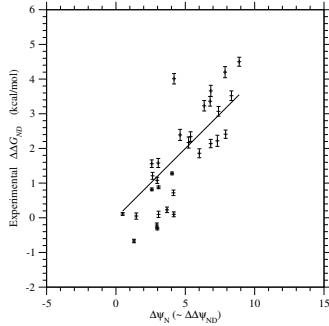


Fig. 16. Regression of the experimental values [65] of folding free energy changes ($\Delta\Delta G_{ND}$) due to single amino acid substitutions on $\Delta\psi_N$ ($\approx \Delta\Delta\psi_{ND}$) for the same types of substitutions in PF00595. The solid line shows the least-squares regression line through the origin with the slope, 0.400 kcal/mol, which is the estimates of $k_B T_s$. The reflective correlation coefficient is equal to 0.92. The free energies are in kcal/mol units.

ous methods [15], [16], [63]. In principle, if folding free energy changes ($\Delta\Delta G_{ND}$) due to single amino acid substitutions are known, the selective temperature T_s can be estimated by comparing $\Delta\Delta G_{ND}$ with $\Delta\Delta\psi_{ND}$, that is, with the equation $\Delta\Delta G_{ND}/(k_B T_s) \approx \Delta\Delta\psi_{ND} \approx \Delta\psi_N$ [16]; see methods S.1.4. In Fig. 16, folding energy changes $\Delta\Delta G_{ND}$ [65] due to single amino acid substitutions in PF00595 are plotted against their evolutionary energy changes $\Delta\psi_N$. The slope of the least-squares regression line through the origin gives the value of $k_B T_s$, 0.400 kcal/mol (201°K) for PF00595.

For protein families for which folding energy changes are unknown, PF00595 may be employed as a reference protein to estimate T_s . The standard deviation of the free energy changes due to single amino acid substitutions, $\overline{Sd(\Delta G_N)}$, must not explicitly depend on $k_B T_s$ but the free energy G_N . On the other hand, the standard deviation of evolutionary energy changes due to single nucleotide nonsynonymous substitutions, $\overline{Sd(\Delta\psi_N)}$, is independent of ψ_N and almost constant across homologous sequences in every protein family as shown in Fig. 17. In other words, $\overline{Sd(\Delta\psi_N)}$ is not a function of G_N but only T_s . Therefore, $\overline{Sd(\Delta G_N)}$ is expected to be nearly constant across protein families [16]; $\overline{Sd(\Delta G_N)} = k_B T_s \overline{Sd(\Delta\psi_N)} \approx \text{constant}$. As a result, T_s can be estimated for any protein family from the ratio of $\overline{Sd(\Delta\psi_N)}$ to

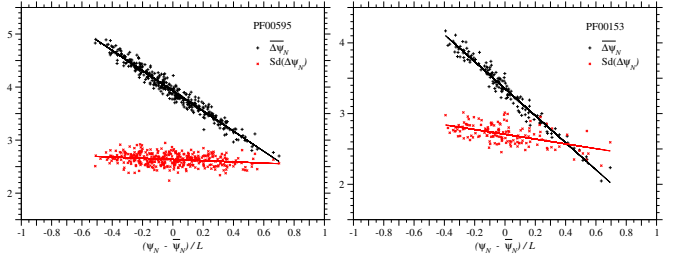


Fig. 17. Relationships between $\Delta\psi_N$ due to single nucleotide nonsynonymous substitutions and ψ_N of the homologous sequences in PF00595 and in PF00153. Each of the black plus and red cross marks corresponds to the mean and the standard deviation of $\Delta\psi_N$ due to all types of single nucleotide nonsynonymous substitutions over all sites in each of the homologous sequences, respectively; the left and right figures are for PF00595 and PF00153, respectively. Representatives of unique sequences with no deletion for PF00595 and with no more than 2 deletions for PF00153, which are at least 20% different from each other, are employed; their numbers are 361 for PF00595 and 144 for PF00153. The solid lines show the regression lines for the mean and the standard deviation of $\Delta\psi_N$. The correlation and regression coefficients are listed in Table 5.

that of a reference protein. The $k_B T_s$ of PF00153 is estimated to be **0.389 kcal/mol (196°K)**. In Table 5, various quantities [16] derived from $\Delta\psi_N$ are listed.

3 DISCUSSION

In the Boltzmann machine learning, the objective function, which is the cross entropy, fluctuates in the minimization process, because the partial derivatives are calculated from the pairwise marginal distributions estimated by MCMC sampling, and the first-order gradient-descent method is also used. The cross entropy, however, cannot be monitored in the minimization process, because it can be hardly evaluated. Here, the average (D_2^{KL}) of Kullback-Leibler divergences for pairwise marginal distributions over all residue pairs is monitored instead as a rough measure of fitting to the reference distribution. As shown in Fig. 2, D_2^{KL} significantly fluctuates in the learning process. On the other hand, the sample and ensemble averages of evolutionary energy smoothly change and slowly converge in the learning process; see Fig. 6. Also, the profile of the sample and ensemble averages of evolutionary energy along the learning process is well reproducible by another run of learning. Here we stop learning

and pick up the parameter estimates corresponding to $\min D_2^{KL}$, if $\min D_2^{KL}$ does not change during a certain number of iterations after a sufficient number of iterations are executed for the sample and ensemble averages of evolutionary energy to converge; see methods S.1.8.3 for details.

Machine learning methods such as Boltzmann machine employ a gradient-descent method to minimize a loss function or cross entropy. There are not a few gradient-descent methods invented. In most machine learning problems, a gradient-descent method is chosen from a view point of the speed and the degree of minimization. Even if there is a unique minimum in an objective function, there can be multiple sets of parameter values that take similarly approximate values for the minimum of the objective function. Some of them may have reasonable characteristics for the solution but the others may not. Thus, we must choose a gradient-descent method that yields reasonable values for parameters. For the present problem, four gradient-descent methods are examined; the Adam method that is commonly employed in machine learning, the RPROP-LR method that is the RPROP modified [14] for Boltzmann machine learnings of protein sequences, and the **ModAdam method that is** the Adam method modified for sparse couplings, and the NAG method that is not a per-parameter learning rate method like the ModAdam but not an adaptive method unlike the ModAdam.

Surprisingly, it is shown in the Boltzmann machine with the L2-L2 regularization for PF00595 that each method gives a very different solution. The Adam method normalizes each partial derivative by a parameter and therefore tend to yield similarly dense interactions even for a sparse-interaction system like protein sequences. On the other hand, the NAG and the ModAdam, in which the stepsize of parameter updates is proportional to the partial gradient and the proportional constant is the same for all parameters, yield the reasonable parameters in which the couplings well correlate with residue-residue distance. This fact strongly indicates that the stepsize must be proportional to the partial gradient to yield reasonable solutions at least for sparse-interaction systems. In other words, the per-parameter methods such as AdaGrad, AdaDelta, RMSprop, and Adam, in which each partial gradient of parameter is normalized, and RPROP, in which the stepsize does not depend on the partial derivative but only on the temporal behavior of its sign, may be appropriate to similarly-dense-interaction systems as well as the L_2 regularization but inappropriate to sparse-interaction systems for which the L_1 regularization is often employed.

On the other hand, the RPROP-LR, in which the stepsize is proportional to the partial derivative, yield similar solutions to the ModAdam, but their profiles of the average evolutionary energies are very different, indicating that in the RPROP-LR convergence is very fast but parameters converge to less favorable interactions to the natural proteins than those inferred by the ModAdam. Also, the RPROP-LR is inferior to the ModAdam in the recoverability of pairwise frequencies.

The results indicate that the profile of the sample and ensemble averages of evolutionary energy is very useful not only for tuning hyper-parameters but also to judge whether iterations of learning converge or not, and which optimization method is better than the others. Although the fields and couplings inferred by the NAG in the L2-L2 almost coincide with those by the ModAdam, the energy profiles indicate that those inferred by the ModAdam are slightly more optimized than those by the NAG.

In the inverse Potts problem, in which the evolutionary inter-

actions, fields and coupling, are inferred from a multiple sequence alignment of protein homologous sequences, regularization must be applied to objective functions in order to prevent over-fitting or to solve ill-posed problems. Commonly used regularizations are L_2 , L_1 and their variants. Regularization, however, introduces hyper-parameters to be determined. In almost all models for protein sequences, regularization parameters have been arbitrarily determined or adjusted to increase the precision for residue-residue contact prediction. In order to correctly infer fields and couplings, however, the other requirement for them should be also taken into account; the sample average of evolutionary energies over target sequences must be equal to the ensemble average. The estimates of the sample and ensemble averages of evolutionary energy significantly depend on regularization parameters as shown in Fig. 1. Here the regularization parameter λ_1 for fields is first tuned as small as possible as long as the sample average of evolutionary energies over target sequences is lower than the ensemble average and both the averages of evolutionary energy decrease. Then, the regularization parameter λ_2 for couplings is tuned as large as possible as long as the sample average of evolutionary energies over target sequences is lower than the ensemble average, where the ensemble average is evaluated by approximating the distribution of the evolutionary energies of random sequences as a Gaussian distribution; the Gaussian approximation [53] is known to be appropriate for native proteins.

The group L_1 regularization was employed for a pseudo-likelihood minimization in a graphical model (GREMLIN [68]) for protein sequences. However, in the inverse Potts problem on protein sequences, most analyses have employed the L_2 regularization because the L_2 function is differentiable, although the L_2 regularization is appropriate to similarly-dense-interaction systems rather than sparse-interaction systems such as protein sequences. The present analyses clearly show that the group L_1 regularization for couplings makes their estimates more sparse and therefore more reasonable than L_1 and L_2 . The present results strongly indicate that regularization models and learning methods must be carefully chosen for particular interaction systems.

The most important question is how precisely the evolutionary interactions can be inferred. Recoverabilities of single-site frequencies and pairwise correlations, and even higher correlations by the inverse Potts model have been examined [12], [13], [14]. On the other hand, reproducibilities of fields and couplings have been examined mostly for artificial systems such as artificial data on Erdős-Renyi models and a lattice protein [12]. Because the reproducibilities of fields and couplings depend on the mode of pairwise interactions, we need to examine how well they can be reproduced for protein sequences. Here the MCMC samples that are generated with the interactions inferred by the Boltzmann machine learning for the natural protein families are employed as protein-like sequences. In other words, fields and couplings are first inferred from protein sequences and compared with those inferred again by Boltzmann machine learning from MCMC samples that are generated with the interactions first inferred. Both the fields and couplings are well recovered for PF00595 and PF00153 except for weak couplings.

However, the distribution of evolutionary energies over the natural proteins significantly shifts towards lower energies in comparison with those over the MCMC samples; see Fig. 15. The same feature was also reported for trypsin inhibitor [12]. This discrepancy is improved if the MCMC samples are employed as protein-like sequences for Boltzmann machine learning; see

Fig. 15. Recovering the pairwise amino acid frequencies in the resolution of a total energy is harder for the natural proteins than for the protein-like sequences.

A computational load is very high for the Boltzmann machine method to infer fields and couplings. Recently, restricted Boltzmann machines that are equivalent to the present Boltzmann machine have been studied [69], [70]. In these models, the coupling interactions $J_{ij}(a_k, a_l)$ are estimated in the decoupled form, $\sum_{\mu=1}^{L_q} \xi_i^\mu(a_k) \xi_j^\mu(a_l)$, and approximated with the small numbers for L_q , reducing a computational load; the number of parameters for coupling interactions may be reduced from $L(L-1)q^2/2$ to LL_qq ; $q = 21$. Thus, using the restricted Boltzmann machines certainly has a merit, although L_q seems to be large to well approximate sparse coupling interactions.

Accurate estimation of coupling interactions is useful in analyses of protein evolution [15], [16] and protein foldings [17], [18]. On the basis of the constancy of the standard deviation of evolutionary energy changes due to single nucleotide nonsynonymous substitutions ($Sd(\Delta\psi_N)$) over protein families, selective temperature, T_s in Eq. S12, was estimated [16] for several proteins from fields and couplings inferred by the mean field DCA method. The estimates of fields and couplings by the mean field DCA method [1], [2] are known to be rough [12], [13]. Therefore, the constancy of $Sd(\Delta\psi_N)$ over protein families has been confirmed here with the present estimates of fields and couplings for PF00595 and PF00153. Although $Sd(\Delta\psi_N)$ are estimated significantly smaller for PF00595 by the Boltzmann machine than that by the mean fields DCA, the methods and discussion [16] on protein evolution are still valid.

The program written in Scala and the MSAs employed are available from <https://gitlab.com/sanzo.miyazawa/BM/>.

REFERENCES

[1] F. Morcos, A. Pagnani, B. Lunt, A. Bertolino, D. S. Marks, C. Sander, R. Zecchina, J. N. Onuchic, T. Hwa, and M. Weigt, "Direct-coupling analysis of residue coevolution captures native contacts across many protein families," *Proc. Natl. Acad. Sci. USA*, vol. 108, pp. E1293–E1301, 2011.

[2] D. S. Marks, L. J. Colwell, R. Sheridan, T. A. Hopf, A. Pagnani, R. Zecchina, and C. Sander, "Protein 3D structure computed from evolutionary sequence variation," *PLoS ONE*, vol. 6, no. 12, p. e28766, 12 2011. [Online]. Available: <http://dx.doi.org/10.1371/journal.pone.0028766>

[3] J. I. Sułkowska, F. Morcos, M. Weigt, T. Hwa, and J. N. Onuchic, "Genomics-aided structure prediction," *Proc. Natl. Acad. Sci. USA*, vol. 109, pp. 10340–10345, 2012.

[4] J. Mout, K. Fidelis, A. Kryshchovych, T. Schwede, and A. Tramontano, "Critical assessment of methods of protein structure prediction: Progress and new directions in round XI," *Proteins*, vol. 84(S1), pp. 4–14, 2016.

[5] S. Ovchinnikov, H. Park, N. Varghese, P.-S. Huang, G. A. Pavlopoulos, D. E. Kim, H. Kamisetty, N. C. Kyrpides, and D. Baker, "Protein structure determination using metagenome sequence data," *Science*, vol. 355, pp. 294–298, 2017.

[6] S. Miyazawa, "Prediction of structures and interactions from genome information," *arXiv:1709.08021 [q-bio.BM]*, 2017.

[7] —, "Prediction of structures and interactions from genome information," in *Integrative Structural Biology with Hybrid Methods*, ser. Advances in Experimental Medicine and Biology 1105, H. Nakamura, Ed. Singapore: Springer Nature Singapore Pte Ltd., 2018, ch. 9.

[8] A. Lapedes, B. Giraud, and C. Jarzynsk, "Using sequence alignments to predict protein structure and stability with high accuracy," *LANL Science Magazine*, vol. LA-UR-02-4481, 2002.

[9] —, "Using sequence alignments to predict protein structure and stability with high accuracy," *arXiv:1207.2484 [q-bio.QM]*, 2012.

[10] M. Ekeberg, C. Lövkvist, Y. Lan, M. Weigt, and E. Aurell, "Improved contact prediction in proteins: Using pseudolikelihoods to infer Potts models," *Phys. Rev. E*, vol. 87, p. 012707, 2013. [Online]. Available: <http://link.aps.org/doi/10.1103/PhysRevE.87.012707>

[11] M. Ekeberg, T. Hartonen, and E. Aurell, "Fast pseudolikelihood maximization for direct-coupling analysis of protein structure from many homologous amino-acid sequences," *J. Comput. Phys.*, vol. 276, pp. 341–356, 2014.

[12] J. P. Barton, E. D. Leonardis, A. Coucke, and S. Cocco, "ACE: adaptive cluster expansion for maximum entropy graphical model inference," *Bioinformatics*, vol. 32, pp. 3089–3097, 2016.

[13] S. Cocco, C. Feinauer, M. Figliuzzi, R. Monasson, and M. Weigt, "Inverse statistical physics of protein sequences: A key issues review," *arXiv:1703.01222 [q-bio.BM]*, 2017.

[14] M. Figliuzzi, P. Barrat-Charlaix, and M. Weigt, "How pairwise coevolutionary models capture the collective residue variability in proteins?" *Mol. Biol. Evol.*, vol. 35, pp. 1018–1027, 2018.

[15] F. Morcos, N. P. Schafer, R. R. Cheng, J. N. Onuchic, and P. G. Wolynes, "Coevolutionary information, protein folding landscapes, and the thermodynamics of natural selection," *Proc. Natl. Acad. Sci. USA*, vol. 111, pp. 12408–12413, 2014.

[16] S. Miyazawa, "Selection originating from protein stability/foldability: Relationships between protein folding free energy, sequence ensemble, and fitness," *J. Theor. Biol.*, vol. 433, pp. 21–38, 2017.

[17] H. Jacquin, A. Gilson, E. Shakhnovich, S. Cocco, and R. Monasson, "Benchmarking inverse statistical approaches for protein structure and design with exactly solvable models," *PLoS Comput. Biol.*, vol. 12, p. e1004889, 2016.

[18] J. P. Barton, A. K. Chakraborty, S. Cocco, H. Jacquin, and R. Monasson, "On the entropy of protein families," *J. Stat. Phys.*, vol. 162, pp. 1267–1293, 2016.

[19] G. E. Hinton and T. J. Sejnowski, "Optimal perceptual inference," *Proceedings of the IEEE conference on Computer Vision and Pattern Recognition*, pp. 448–453, 1983.

[20] A. D. H., H. G. E., and S. T. J., "A learning algorithm for boltzmann machines," *Cogn. Sci.*, vol. 9, pp. 147–169, 1985.

[21] G. E. Hinton, "Boltzmann machine," *Scholarpedia*, vol. 2, p. 1668, 2007.

[22] M. Weigt, R. A. White, H. Szurmant, J. A. Hoch, and T. Hwa, "Identification of direct residue contacts in protein-protein interaction by message passing," *Proc. Natl. Acad. Sci. USA*, vol. 106, pp. 67–72, 2009.

[23] N. Metropolis, A. W. Rosenbluth, M. N. Rosenbluth, A. H. Teller, and E. Teller, "Equation of state calculations by fast computing machines," *J. Chem. Phys.*, vol. 21, pp. 1087–1092, 1953.

[24] W. K. Hastings, "Monte carlo sampling methods using markov chains and their applications," *Biometrika*, vol. 57, pp. 97–109, 1970.

[25] S. Geman and D. Geman, "Stochastic relaxation, gibbs distributions, and the bayesian restoration of images," *IEEE Trans. Pattern Anal. Mach. Intell.*, 1984.

[26] A. S. Lapedes, B. G. Giraud, L. C. Liu, and G. D. Stormo, "Correlated mutations in protein sequences: phylogenetic and structural effects," in *IMS Lecture Notes: Statistics in Molecular Biology and Genetics: Selected Proceedings of the Joint AMS-IMS-SIAM Summer Conference on Statistics in Molecular Biology, June 22-26, 1997*, F. Seillier-Moiseiwitsch, Ed. Institute of Mathematical Statistics, 1999, pp. 345–352.

[27] W. P. Russ, D. M. Lowery, P. Mishra, M. B. Yaffe, and R. Ranganathan, "Natural-like function in artificial WW domains," *Nature*, vol. 437, pp. 579–583, 2005.

[28] J. M. Skerker, B. S. Perchuk, A. Siryaporn, E. A. Lubin, O. Ashenberg, M. Goulian, and M. T. Laub, "Rewiring the specificity of two-component signal transduction systems," *Cell*, vol. 133, pp. 1043–1054, 2008.

[29] L. Burger and E. van Nimwegen, "Accurate prediction of protein-protein interactions from sequence alignments using a Bayesian method," *Mol. Syst. Biol.*, vol. 4, p. 165, 2008.

[30] N. Halabi, O. Rivoire, S. Leibler, and R. Ranganathan, "Protein sectors: evolutionary units of three-dimensional structure," *Cell*, vol. 138, pp. 774–786, 2009.

[31] L. Burger and E. van Nimwegen, "Disentangling direct from indirect co-evolution of residues in protein alignments," *PLoS Comput. Biol.*, vol. 6, no. 1, p. e1000633, 01 2010. [Online]. Available: <http://dx.doi.org/10.1371/journal.pcbi.1000633>

[32] D. Altschuh, T. Vernet, P. Berti, D. Moras, and K. Nagai, "Coordinated amino acid changes in homologous protein families," *Protein Eng.*, vol. 2, pp. 193–199, 1988.

[33] U. Göbel, C. Sander, R. Schneider, and A. Valencia, "Correlated mutations and residue contacts in proteins," *Proteins*, vol. 18, pp. 309–317, 1994.

- [34] I. N. Shindyalov, N. A. Kolchanov, and C. Sander, "Can three-dimensional contacts in protein structures be predicted by analysis of correlated mutations?" *Protein Eng.*, vol. 7, pp. 349–358, 1994.
- [35] D. D. Pollock and W. R. Taylor, "Effectiveness of correlation analysis in identifying protein residues undergoing correlated evolution," *Protein Eng.*, vol. 10, pp. 647–657, 1997.
- [36] D. D. Pollock, W. R. Taylor, and N. Goldman, "Coevolving protein residues: maximum likelihood identification and relationship to structure," *J. Mol. Biol.*, vol. 287, pp. 187–198, 1999.
- [37] W. R. Atchley, K. R. Wollenberg, W. M. Fitch, W. Terhalle, and A. W. Dress, "Correlations among amino acid sites in bHLH protein domains: an information theoretic analysis," *Mol. Biol. Evol.*, vol. 17, pp. 164–178, 2000.
- [38] P. Fariselli, O. Olmea, A. Valencia, and R. Casadio, "Prediction of contact maps with neural networks and correlated mutations," *Protein Eng.*, vol. 14, pp. 835–843, 2001.
- [39] A. A. Fodor and R. W. Aldrich, "Influence of conservation on calculations of amino acid covariance in multiple sequence alignment," *Proteins*, vol. 56, pp. 211–221, 2004.
- [40] S. J. Fleishman, O. Yifrach, and N. Ben-Tal, "An evolutionarily conserved network of amino acids mediates gating in voltage-dependent potassium channels," *J. Mol. Biol.*, vol. 340, pp. 307–318, 2004.
- [41] J. Duthel, T. Pupko, A. Jean-Marie, and N. Galtier, "A model-based approach for detecting coevolving positions in a molecule," *Mol. Biol. Evol.*, vol. 22, pp. 1919–1928, 2005.
- [42] L. C. Martin, G. B. Gloor, S. D. Dunn, and L. M. Wahl, "Using information theory to search for co-evolving residues in proteins," *Bioinformatics*, vol. 21, pp. 4116–4124, 2005.
- [43] M. Fares and S. Travers, "A novel method for detecting intramolecular coevolution," *Genetics*, vol. 173, pp. 9–23, 2006.
- [44] A. Doron-Faigenboim and T. Pupko, "A combined empirical and mechanistic codon model," *Mol. Biol. Evol.*, vol. 24, pp. 388–397, 2007.
- [45] J. Duthel and N. Galtier, "Detecting groups of coevolving positions in a molecule: a clustering approach," *BMC Evol. Biol.*, vol. 7, p. 242, 2007.
- [46] S. D. Dunn, L. M. Wahl, and G. B. Gloor, "Mutual information without the influence of phylogeny or entropy dramatically improves residue contact prediction," *Bioinformatics*, vol. 24, pp. 333–340, 2008.
- [47] A. F. Y. Poon, F. I. Lewis, S. D. W. Frost, and S. L. Kosakovsky Pond, "Spidermonkey: rapid detection of co-evolving sites using Bayesian graphical models," *Bioinformatics*, vol. 24, pp. 1949–1950, 2008.
- [48] J. Duthel, "Detecting coevolving positions in a molecule: why and how to account for phylogeny," *Brief. Bioinform.*, vol. 13, pp. 228–243, 2012.
- [49] A. Gulyás-Kovács, "Integrated analysis of residue coevolution and protein structure in ABC transporters," *PLoS ONE*, vol. 7, no. 5, p. e36546, 05 2012. [Online]. Available: <http://dx.doi.org/10.1371/journal.pone.0036546>
- [50] E. I. Shakhnovich and A. M. Gutin, "A new approach to the design of stable proteins," *Protein Eng.*, vol. 6, pp. 793–800, 1993.
- [51] —, "Engineering of stable and fast-folding sequences of model proteins," *Proc. Natl. Acad. Sci. USA*, vol. 90, pp. 7195–7199, 1993.
- [52] S. Ramanathan and E. Shakhnovich, "Statistical mechanics of proteins with evolutionary selected sequences," *Phys. Rev. E*, vol. 50, pp. 1303–1312, 1994.
- [53] V. S. Pande, A. Y. Grosberg, and T. Tanaka, "Statistical mechanics of simple models of protein folding and design," *Biophys. J.*, vol. 73, pp. 3192–3210, 1997.
- [54] H. Zou and T. Hastie, "Regularization and variable selection via the elastic net," *J. Royal Stat. Soc. Series B*, vol. 67, pp. 301–320, 2005.
- [55] D. E. Rumelhart, G. E. Hinton, and R. J. Williams, "Learning representations by back-propagating errors," *Nature*, vol. 323, pp. 533–536, 1986.
- [56] Y. Nesterov, *Introductory Lectures on Convex Optimization. A Basic Course*. New York: Springer, 2004.
- [57] J. Duchi, E. Hazan, and Y. Singer, "Adaptive subgradient methods for online learning and stochastic optimization," *J. Mach. Learn. Res.*, vol. 12, pp. 2121–2159, 2011.
- [58] M. D. Zeiler, "ADADELTA: An adaptive learning rate method," *arXiv:1212.5701*, 2012.
- [59] M. Riedmiller and H. Braun, "A direct adaptive method for faster backpropagation learning: the RPROP algorithm," *IEEE International Conference on Neural Networks*, pp. 586–591, 1993.
- [60] M. Riedmiller, "Advanced supervised learning in multi-layer perceptrons - from backpropagation to adaptive learning algorithms," *Computer Standards and Interfaces*, vol. 16, pp. 265–278, 1994.
- [61] T. Tieleman and G. Hinton, "Lecture 6.5-rmsprop: Divide the gradient by a running average of its recent magnitude," *COURSERA: Neural Networks for Machine Learning*, 2012.
- [62] D. P. Kingma and J. L. Ba, "Adam: A method for stochastic optimization," *arXiv:1412.6980*, 2014.
- [63] N. V. Dokholyan and E. I. Shakhnovich, "Understanding hierarchical protein evolution from first principles," *J. Mol. Biol.*, vol. 312, pp. 289–307, 2001.
- [64] S. El-Gebali, J. Mistry, A. Bateman, S. R. Eddy, A. Luciani, S. C. Potter, M. Qureshi, L. J. Richardson, G. A. Salazar, A. Smart, E. L. Sonnhammer, L. Hirsh, L. Paladin, D. Piovesan, S. C. Tosatto, and R. D. Finn, "The Pfam protein families database in 2019," *Nucl. Acid Res.*, vol. 47, pp. D427–D432, 2019.
- [65] S. Gianni, C. D. Geierhaas, N. Calosci, P. Jemth, G. W. Vuister, C. Travaglini-Allocatelli, M. Vendruscolo, and M. Brunori, "A PDZ domain recapitulates a unifying mechanism for protein folding," *Proc. Natl. Acad. Sci. USA*, vol. 104, pp. 128–133, 2007.
- [66] G. M. Torchio, M. R. Ermácora, and M. P. Sica, "Equilibrium unfolding of the PDZ domain of β 2-syntrophin," *Biophys. J.*, vol. 102, pp. 2835–2844, 2012.
- [67] S. Gianni, N. Calosci, J. M. A. Aelen, G. W. Vuister, M. Brunori, and C. Travaglini-Allocatelli, "Kinetic folding mechanism of PDZ2 from PTP-BL," *Protein Eng. Design Selection*, vol. 18, pp. 389–395, 2005.
- [68] S. Balakrishnan, H. Kamisetty, J. G. Carbonell, S. I. Lee, and C. J. Langmead, "Learning generative models for protein fold families," *Proteins*, vol. 79, pp. 1061–1078, 2011.
- [69] J. Tubiana, S. Cocco, and R. Monasson, "Learning protein constitutive motifs from sequence data," *eLife*, vol. 8, p. e39397, 2019.
- [70] K. Shimagaki and M. Weigt, "Selection of sequence motifs and generative hopfield-potts models for protein families," *Phys. Rev. E*, vol. 100, p. 032128, 2019.
- [71] S. Miyazawa, "Prediction of contact residue pairs based on co-substitution between sites in protein structures," *PLoS ONE*, vol. 8, no. 1, p. e54252, 01 2013. [Online]. Available: <http://dx.doi.org/10.1371/journal.pone.0054252>
- [72] C. Baldassi, M. Zamparo, C. Feinauer, A. Procaccini, R. Zecchina, M. Weigt, and A. Pagnani, "Fast and accurate multivariate Gaussian modeling of protein families: Predicting residue contacts and protein-interaction partners," *PLoS ONE*, vol. 9, no. 3, p. e92721, 03 2014. [Online]. Available: <https://dx.doi.org/10.1371/journal.pone.0092721>
- [73] H. Kamisetty, S. Ovchinnikov, and D. Baker, "Assessing the utility of coevolution-based residue-residue contact predictions in a sequence- and structure-rich era," *Proc. Natl. Acad. Sci. USA*, vol. 110, pp. 15 674–15 679, 2013.
- [74] S. Miyazawa and R. L. Jernigan, "Equilibrium folding and unfolding pathways for a model protein," *Biopolymers*, vol. 21, pp. 1333–1363, 1982.
- [75] C. De Mol, E. De Vito, and L. Rosasco, "Elastic-net regularization in learning theory," *J. Complexity*, vol. 25, pp. 201–230, 2009.
- [76] S. Mosci, L. Rosasco, S. Matteo, A. Verri, and S. Villa, "Solving structured sparsity regularization with proximal methods," *Machine Learning and Knowledge Discovery in Databases*, vol. 6322, pp. 418–433, 2010.
- [77] M. Schmidt, "CPSC 540: Machine learning; group L1-regularization, proximal-gradient," 2017. [Online]. Available: <https://www.cs.ubc.ca/~schmidtm/Courses/540-W17/L5.pdf>



Sanzo Miyazawa had worked for the Graduate School of Engineering in Gunma University, Japan until retired at age 65 in 2013. His research interests include protein structure and evolution.

Supplementary Material
for
Boltzmann Machine Learning and Regularization Methods for Inferring
Evolutionary Fields and Couplings from a Multiple Sequence Alignment
(Article DOI: 10.1109/TCBB.2020.2993232)
in
IEEE/ACM Transactions on Computational Biology and Bioinformatics, 2020

Sanzo Miyazawa
sanzo.miyazawa@gmail.com

2021-06-07

S.1 METHODS

S.1.1 The Inverse Potts model for protein homologous sequences

Let us consider probability distributions $P(\sigma)$ of amino acid sequences $\sigma \equiv (\sigma_1, \dots, \sigma_L)$, which satisfy the following constraints that single-site and two-site marginal probabilities must be equal to a given frequency $P_i(a_k)$ of amino acid a_k at each site i and a given frequency $P_{ij}(a_k, a_l)$ of amino acid pair (a_k, a_l) for site pair (i, j) , respectively.

$$P(\sigma_i = a_k) \equiv \sum_{\sigma} P(\sigma) \delta_{\sigma_i a_k} = P_i(a_k) \quad (S1)$$

$$P(\sigma_i = a_k, \sigma_j = a_l) \equiv \sum_{\sigma} P(\sigma) \delta_{\sigma_i a_k} \delta_{\sigma_j a_l} = P_{ij}(a_k, a_l) \quad (S2)$$

where $\sigma_i, a_k \in \{\text{amino acids, deletion}\}$ $k = 1, \dots, q$, $q \equiv |\{\text{amino acids, deletion}\}| = 21$, $i, j = 1, \dots, L$, and $\delta_{\sigma_i a_k}$ is the Kronecker delta. The sequence distribution $P(\sigma|h, J)$ with the maximum entropy can be represented as

$$P(\sigma|h, J) = \frac{1}{Z_{\sigma}} e^{-\psi_N(\sigma|h, J)} \quad , \quad Z_{\sigma} = \sum_{\sigma} e^{-\psi_N(\sigma|h, J)} \quad (S3)$$

$$\psi_N(\sigma|h, J) = - \left[\sum_i \{ h_i(\sigma_i) + \sum_{j(>i)} J_{ij}(\sigma_i, \sigma_j) \} \right] \quad (S4)$$

where Lagrange multipliers $h_i(a_k)$ and $J_{ij}(a_k, a_l)$ are interaction potentials called fields and couplings, and $\psi_N(\sigma|h, J)$ is referred to here as evolutionary energy.

Fields $h_i(a_k)$ and couplings $J_{ij}(a_k, a_l)$ provide useful information to understand protein evolution [16] and also to predict residue-residue contacts in protein structures on the basis of coevolutional residue substitutions [1], [2], [8], [71].

For given single-site $P_i(a_k)$ and two-site frequencies $P_{ij}(a_k, a_l)$, which are evaluated from a multiple sequence alignment, inferring $h_i(a_k)$ and $J_{ij}(a_k, a_l)$ have been attempted as the Inverse Potts problem by the Boltzmann machine learning [14], [22], by the mean field approximation [1], [2], [8], by the Gaussian approximation [72], by maximizing a pseudo-likelihood [10], [11], [68], [73], and by minimizing a cross entropy in the adaptive cluster expansion [12].

S.1.2 The sample average of evolutionary energy

According to the Potts model, the sample average of $\psi_N(\sigma_N)$ over natural sequences, σ_N , fixed in protein evolution is equal to the ensemble average of $\psi_N(\sigma)$ over sequences, σ . Sample averages are calculated with a sample weight w_{σ_N} for each homologous sequence, which is used to reduce phylogenetic biases in the set of homologous sequences; for example, the sample average of evolutionary energy is calculated as follows.

$$\overline{\psi_N(\sigma_N)} \equiv \frac{\sum_{\sigma_N} w_{\sigma_N} \psi_N(\sigma_N)}{\sum_{\sigma_N} w_{\sigma_N}} \quad (S5)$$

$$= \langle \psi_N(\sigma) \rangle_{\sigma} \quad (S6)$$

where $\overline{\psi_N(\sigma_N)}$ denotes a sample average of $\psi_N(\sigma_N)$ with a sample weight w_{σ_N} for each homologous sequence σ_N , and $\langle \psi_N(\sigma) \rangle_{\sigma}$ is the ensemble average of $\psi_N(\sigma)$ that obeys a Boltzmann distribution.

S.1.3 Ensemble average by a Gaussian Approximation for the distribution of the evolutionary energies of random sequences

The ensemble average over sequences, for example, of $\psi_N(\sigma)$ is estimated by the Gaussian approximation [16], [53], in which the distribution of the evolutionary energies of random sequences is approximated as a Gaussian distribution, $\mathcal{N}(\bar{\psi}, \delta\psi^2)$. The mean $\bar{\psi}$ and variance $\delta\psi^2$ are evaluated as those of evolutionary energies of random sequences whose amino acid composition is equal to the average amino acid composition of sequences in a protein family.

$$\langle \psi_N(\sigma) \rangle_{\sigma} \equiv \left[\sum_{\sigma} \psi_N(\sigma) \exp(-\psi_N(\sigma)) \right] / Z_{\sigma} \quad (S7)$$

$$\approx \frac{\int \psi_N \exp(-\psi_N) \mathcal{N}(\bar{\psi}, \delta\psi^2) d\psi_N}{\int \exp(-\psi_N) \mathcal{N}(\bar{\psi}, \delta\psi^2) d\psi_N} \quad (S8)$$

$$= \bar{\psi}(\overline{f(\sigma_N)}) - \delta\psi^2(\overline{f(\sigma_N)}) \quad (S9)$$

where $\overline{f(\sigma_N)}$ is the sample-average amino acid composition of natural sequences in a protein family.

S.1.4 Relationships between evolutionary energy $\psi_N(\sigma)$, fitness $m(\sigma)$, and folding free energy $\Delta G_{ND}(\sigma)$ of protein σ [16]

In [16], it was proved by assuming the detailed balance principle that the equilibrium distribution of protein sequences must be the Boltzmann distribution of their Malthusian fitness m as well as that of $\Delta\psi_{ND}$. On the other hand, a protein folding theory [50], [51], [52], [53] based on a random energy model (REM) indicates that it can be approximated to the Boltzmann distribution of the folding free energy divided by selective temperature, $\Delta G_{ND}/(k_B T_s)$.

$$P^{\text{eq}}(\mu) = \frac{P^{\text{mut}}(\mu) \exp(4N_e m(\mu)(1 - q_m))}{\sum_{\nu} P^{\text{mut}}(\nu) \exp(4N_e m(\nu)(1 - q_m))} \quad (S10)$$

$$= \frac{P^{\text{mut}}(\bar{\mu}) \exp(-(\psi_N(\mu) - \psi_D(\bar{f}(\mu), T)))}{\sum_{\nu} P^{\text{mut}}(\bar{\nu}) \exp(-(\psi_N(\nu) - \psi_D(\bar{f}(\nu), T)))} \quad (S11)$$

$$\approx \frac{P^{\text{mut}}(\mu) \exp(-\Delta G_{ND}(\mu, T)/(k_B T_s))}{\sum_{\nu} P^{\text{mut}}(\nu) \exp(-\Delta G_{ND}(\nu, T)/(k_B T_s))} \quad (S12)$$

where $p^{\text{mut}}(\sigma)$ is the probability of a sequence (σ) randomly occurring in a mutational process and depends only on the amino acid composition of the sequence $f(\sigma)$, q_m is the frequency of a single mutant gene in a population, k_B is the Boltzmann constant, T is growth temperature, T_s is selective temperature that quantifies how strong the folding constraints are in protein evolution, $f(\sigma) \equiv \sum_{\sigma} f(\sigma) P(\sigma)$ and $\log P^{\text{mut}}(\bar{\sigma}) \equiv \sum_{\sigma} P(\sigma) \log(\prod_i P^{\text{mut}}(\sigma_i))$. Then, the following relationships are derived for sequences for which $f(\mu) = \bar{f}(\mu)$.

$$4N_e m(\mu)(1 - q_m) = -\Delta\psi_{ND}(\mu, T) + \text{constant} \quad (S13)$$

$$\approx \frac{-\Delta G_{ND}(\mu, T)}{k_B T_s} + \text{constant} \quad (S14)$$

The selective advantage of ν to μ is represented as follows for $f(\mu) = \bar{f}(\nu) = \bar{f}(\sigma)$.

$$4N_e s(\mu \rightarrow \nu)(1 - q_m) = (4N_e m(\nu) - 4N_e m(\mu))(1 - q_m) \quad (S15)$$

$$= -(\Delta\psi_{ND}(\nu, T) - \Delta\psi_{ND}(\mu, T)) = -(\psi_N(\nu) - \psi_N(\mu)) \quad (S16)$$

$$\approx -(\Delta G_{ND}(\nu, T) - \Delta G_{ND}(\mu, T))/(k_B T_s) = -(G_N(\nu) - G_N(\mu))/(k_B T_s) \quad (S17)$$

$$\psi_N(\mu) \approx G_N(\mu)/(k_B T_s) \quad \psi_D(\mu) \approx G_D(\mu)/(k_B T_s) \quad (S18)$$

where $G_N(\sigma)$ and $G_D(\sigma)$ are the free energies of the native and the denatured states of sequence σ . It should be noted here that only sequences for which $f(\sigma) = \bar{f}(\sigma)$ contribute significantly to the partition functions in Eq. S11, and other sequences may be ignored.

S.1.5 Relationships among selective temperature (T_s), glass transition temperature (T_g), and melting temperature (T_m) of protein

The distribution of conformational energies in the denatured state (molten globule state), which consists of conformations as compact as the native conformation, is approximated in the random energy model (REM), particularly the independent interaction model (IIM) [53], to be equal to the energy distribution of the randomized sequences, which is approximated by the energy distribution of the random sequences with the same amino acid composition and then by a Gaussian distribution, in the native conformation. That is, the partition function Z for the denatured state is written as follows with the number density per energy $n(E)$ of conformations that is approximated by a product of a Gaussian probability density and the total number of conformations whose logarithm is proportional to the chain length.

$$Z = \int \exp\left(\frac{-E}{k_B T}\right) n(E) dE \quad (S19)$$

$$n(E) \approx \exp(\omega L) \mathcal{N}(\bar{E}(\mathbf{f}(\sigma_N)), \delta E^2(\mathbf{f}(\sigma_N))) \quad (S20)$$

where ω is the conformational entropy per residue in the compact denatured state, and $\mathcal{N}(\bar{E}(\mathbf{f}(\sigma_N)), \delta E^2(\mathbf{f}(\sigma_N)))$ is the Gaussian probability density with mean \bar{E} and variance δE^2 , which depend only on the amino acid composition, $\mathbf{f}(\sigma_N)$, of the protein sequence, σ_N . The free energy of the denatured state is approximated as follows.

$$G_D(\sigma_N, T) \approx \bar{E}(\mathbf{f}(\sigma_N)) - \frac{\delta E^2(\mathbf{f}(\sigma_N))}{2k_B T} - k_B T \omega L \quad (S21)$$

$$= \bar{E}(\mathbf{f}(\sigma_N)) - \delta E^2(\mathbf{f}(\sigma_N)) \frac{\vartheta(T/T_g)}{k_B T} \quad (S22)$$

$$\psi_D(\sigma_N, T) \approx \bar{\psi}(\mathbf{f}(\sigma)) - \delta \psi^2(\mathbf{f}(\sigma)) \vartheta(T/T_g) \frac{T_s}{T} \quad (S23)$$

$$\vartheta\left(\frac{T}{T_g}\right) \equiv (1 + T^2/T_g^2)/2 \quad \text{for } T \geq T_g \quad (S24)$$

where $\bar{E}(\bar{\psi})$ and $\delta E^2(\delta \psi^2)$ are estimated as the mean and variance of interaction energies $E(\psi_N)$ of the randomized sequences, which are approximated by random sequences, in the native conformation; $\bar{E} \simeq k_B T_s \bar{\psi}$ and $\delta E^2 \simeq (k_B T_s)^2 \delta \psi^2$. T_g is the glass transition temperature of the protein at which entropy becomes zero [50], [51], [52], [53].

$$-\frac{\partial G_D}{\partial T} \Big|_{T=T_g} = 0 \quad (S25)$$

The conformational entropy per residue ω in the compact denatured state can be represented with T_g .

$$\omega L = \frac{\delta E^2}{2(k_B T_g)^2} \quad (S26)$$

Thus, unless $T_g < T_m$, a protein will be trapped at local minima on a rugged free energy landscape before it can fold into a unique native structure.

The ensemble average of $\Delta G_{ND}(\sigma, T)$ over sequences, which is observable as the sample averages of $\Delta G_{ND}(\sigma_N, T)$ over homologous sequences fixed in protein evolution, is estimated as follows [16].

$$\begin{aligned} \langle \Delta G_{ND}(\sigma, T) \rangle_\sigma &\equiv \sum_{\sigma} \Delta G_{ND}(\sigma, T) P^{\text{eq}}(\sigma) \\ &\approx \sum_{\{\sigma | f(\sigma) = \bar{f}(\sigma_N)\}} \Delta G_{ND}(\sigma, T) P^{\text{eq}}(\sigma) \quad (S27) \end{aligned}$$

$$= \langle G_N(\sigma) \rangle_\sigma - G_D(\bar{\mathbf{f}}(\sigma_N), T) \quad (S28)$$

where the ensemble averages of $G_N(\sigma)$ over sequences is also estimated in the Gaussian approximation [53].

$$\begin{aligned} \langle G_N(\sigma) \rangle_\sigma &\approx \int E \exp\left(-\frac{E}{k_B T_s}\right) \mathcal{N}(\bar{E}(\mathbf{f}(\sigma_N)), \delta E^2(\mathbf{f}(\sigma_N))) dE \quad (S29) \end{aligned}$$

$$= \bar{E}(\mathbf{f}(\sigma_N)) - \frac{\delta E^2(\mathbf{f}(\sigma_N))}{k_B T_s} \quad (S30)$$

The sample averages of $\Delta G_{ND}(\sigma_N, T)$ and $\psi_N(\sigma_N)$ over homologous sequences fixed in protein evolution are equal to their ensemble averages over sequences [16].

$$\begin{aligned} \overline{\Delta G_{ND}(\sigma_N, T)/(k_B T_s)} &= \langle \Delta G_{ND}(\sigma, T) \rangle_\sigma / (k_B T_s) \quad (S31) \end{aligned}$$

$$\approx [\delta E^2(\mathbf{f}(\sigma_N)) [\vartheta(T/T_g) T_s / T - 1] / (k_B T_s)^2] \quad (S32)$$

$$= \delta \psi^2(\mathbf{f}(\sigma_N)) [\vartheta(T/T_g) T_s / T - 1] \quad (S33)$$

$$= \overline{\Delta G_{ND}(\sigma_N, T_g)} / (k_B T_s') \quad (S34)$$

$$T_s' = T_s (T_s / T_g - 1) / (\vartheta(T/T_g) T_s / T - 1) \quad (S35)$$

$$\overline{\psi_N(\sigma_N)} \equiv \frac{\sum_{\sigma_N} w_{\sigma_N} \psi_N(\sigma_N)}{\sum_{\sigma_N} w_{\sigma_N}} \quad (S36)$$

$$= \langle \psi_N(\sigma) \rangle_\sigma \approx \bar{\psi}(\mathbf{f}(\sigma_N)) - \delta \psi^2(\mathbf{f}(\sigma_N)) \quad (S37)$$

where the sample averages are calculated with a sample weight w_{σ_N} for each homologous sequence, which is used to reduce phylogenetic biases in the set of homologous sequences. $\Delta G_{ND}(\sigma_N, T_g)$ corresponds to the energy gap [50] between the native and the glass states, and T_s' will be the selective temperature if $\Delta G_{ND}(\sigma_N, T_g)$ is used for selection instead of $\Delta G_{ND}(\sigma_N, T)$.

The folding free energy becomes equal to zero at the melting temperature T_m ; $\langle \Delta G_{ND}(\sigma_N, T_m) \rangle_\sigma = 0$. Thus, the following relationship must be satisfied [50], [51], [52], [53].

$$\vartheta\left(\frac{T_m}{T_g}\right) \frac{T_s}{T_m} = \frac{T_s}{2T_m} \left(1 + \frac{T_m^2}{T_g^2}\right) = 1 \quad \text{with } T_s \leq T_g \leq T_m \quad (S38)$$

S.1.6 Boltzmann machine learning

The cross entropy with a regularization term, S , which corresponds to a negative log-posterior-probability per instance, is minimized.

$$S \equiv -\frac{1}{\sum_{\tau} 1} \sum_{\tau} \log P(\sigma^\tau) + R \quad (S39)$$

where R is a regularization term, and τ denotes an instance. According to [14], instead of h_i and J_{ij} , we use the new parameters ϕ_i and ϕ_{ij} for minimization, which are Lagrange multipliers in the maximum entropy model corresponding to $[\sum_{\sigma} P(\sigma) \delta_{\sigma, a_k} - P_i(a_k)]$ and $[\sum_{\sigma} P(\sigma) \delta_{\sigma, a_k} \delta_{\sigma, a_l} - P_{ij}(a_k, a_l) - \sum_{\sigma} P(\sigma) \delta_{\sigma, a_k} P_j(a_l) - P_i(a_k) \sum_{\sigma} P(\sigma) \delta_{\sigma, a_l} + 2P_i(a_k) P_j(a_l)]$ in the

maximum entropy model, respectively. The partial derivatives of the cross entropy can be easily calculated:

$$\frac{\partial S}{\partial \phi_i(a_k)} = \sum_{\sigma} P(\sigma) \delta_{\sigma_i a_k} - P_i(a_k) + \frac{\partial R}{\partial \phi_i(a_k)} \quad (\text{S40})$$

$$\begin{aligned} \frac{\partial S}{\partial \phi_{ij}(a_k, a_l)} &= \left[\sum_{\sigma} P(\sigma) \delta_{\sigma_i a_k} \delta_{\sigma_j a_l} - P_{ij}(a_k, a_l) \right. \\ &\quad \left. - \sum_{\sigma} P(\sigma) \delta_{\sigma_i a_k} P_j(a_l) - P_i(a_k) \sum_{\sigma} P(\sigma) \delta_{\sigma_j a_l} \right. \\ &\quad \left. + 2P_i(a_k) P_j(a_l) \right] + \frac{\partial R}{\partial \phi_{ij}(a_k, a_l)} \end{aligned} \quad (\text{S41})$$

The relationships between (h_i, J_{ij}) and (ϕ_i, ϕ_{ij}) are as follows.

$$h_i(a_k) = \phi_i(a_k) - \sum_{j(\neq i)} \sum_l \phi_{ij}(a_k, a_l) P_j(a_l) \quad (\text{S42})$$

$$J_{ij}(a_k, a_l) = \phi_{ij}(a_k, a_l) \quad (\text{S43})$$

The single-site and two-site frequencies, $P_i(a_k)$ and $P_{ij}(a_k, a_l)$, are evaluated from homologous sequences, each of which has a sample weight w_{σ_N} , in a multiple sequence alignment.

$$P_i(a_k) = \frac{\sum_{\sigma_N} w_{\sigma_N} \delta_{\sigma_N i a_k}}{\sum_{\sigma_N} w_{\sigma_N}} \quad (\text{S44})$$

$$P_{ij}(a_k, a_l) = \frac{\sum_{\sigma_N} w_{\sigma_N} \delta_{\sigma_N i a_k} \delta_{\sigma_N j a_l}}{\sum_{\sigma_N} w_{\sigma_N}} \quad (\text{S45})$$

where σ_N denotes natural sequences.

$\sum_{\sigma} P(\sigma) \delta_{\sigma_i a_k}$ and $\sum_{\sigma} P(\sigma) \delta_{\sigma_i a_k} \delta_{\sigma_j a_l}$ are estimated by a Markov chain Monte Carlo method with the Metropolis-Hastings algorithm [23], [24], and then a gradient-descent algorithm is used to minimize the cross entropy S ; the Metropolis-Hastings algorithm was employed rather than the Gibbs sampler [25], because calculating full conditionals require more computation time.

S.1.7 Regularization

Couplings $\phi_{ij}(a_k, a_l)$ are expected to be significant between residues that are closely located in a 3D protein structure and complex. Thus, they are expected to be sparse, because the number of residue-residue contacts in a protein 3D structure is between 2 and 4 per residue depending on a criterion, in comparison with the number of residue pairs, $L(L-1)/2$, where L is a protein length [74]. Here, to take account of the sparsity of the couplings, the elastic net [54], [75], [76] and group L_1 regularizations are employed to see the effects of different regularizations. The elastic net regularization [54], [75], [76] is used instead of pure L_1 regularization, which is not strictly convex and can occasionally produce non-unique solutions [54]. Group L_1 is employed to deal with pairwise couplings, $\phi_{ij}(a_k, a_l)$, between residues i and j as a group.

S.1.7.1 An elastic net regularization

An elastic net regularization [54], [75], [76] is a mixture of L_1 and L_2 .

$$\begin{aligned} R &\equiv \lambda_1 \sum_i \sum_k \{ \theta_1 |\phi_i(a_k)| + \frac{(1-\theta_1)}{2} \phi_i(a_k)^2 \} + \\ &\quad \lambda_2 \sum_i \sum_k \sum_{j(>i)} \sum_l \{ \theta_2 |\phi_{ij}(a_k, a_l)| + \frac{(1-\theta_2)}{2} \phi_{ij}(a_k, a_l)^2 \} \end{aligned} \quad (\text{S46})$$

where $0 \leq \theta_1 \leq 1$ and $0 \leq \theta_2 \leq 1$. If $\theta = 0(1)$, the regularization will be $L_2(L_1)$. In the present work, L_1 regularization means the elastic net with $\theta = 0.9$ rather than 1.0.

S.1.7.1.1 The soft-thresholding function for L_1 regularization: Let us assume that the learning of fields and couplings (ϕ_i, ϕ_{ij}) is iteratively updated as follows.

$$\phi_{\mu}(t+1) = \phi_{\mu}(t) - [\alpha_{\mu}(t+1) + \beta_{\mu}(t+1) \left(\frac{\partial S}{\partial \phi_{\mu}} \right)_{\phi(t)}] \quad (\text{S47})$$

$$= \phi_{\mu}(t+1 \text{ without } L_1) - \gamma_{\mu}(t+1) \left(\frac{\partial |\phi_{\mu}|}{\partial \phi_{\mu}} \right)_{\phi(t)} \quad (\text{S48})$$

$$= \text{prox}(\gamma_{\mu}(t+1) |\phi_{\mu}|, \phi_{\mu}(t+1 \text{ without } L_1)) \quad (\text{S49})$$

where the suffix μ denotes $_i(a_k)$ or $_{ij}(a_k, a_l)$, $\phi_{\mu}(t+1 \text{ without } L_1)$ is $\phi_{\mu}(t+1)$ which does not include the L_1 regularization term, and the second term is one corresponding to the L_1 terms of the regularization in Eq. S46, and the derivative in the second term may be evaluated as a subderivative at a singular point. Here the proximal operator [77] defined as follows is used for faster convergence.

$$\text{prox}(h(u), x) \equiv \underset{u}{\text{argmin}} (h(u) + \frac{1}{2} \|u - x\|_2^2) \quad (\text{S50})$$

The proximal operator for L_1 regression is equal to:

$$\begin{aligned} &\text{prox}(\gamma_{\mu}(t+1) |\phi_{\mu}|, \phi_{\mu}(t+1 \text{ without } L_1)) \\ &= \underset{\phi_{\mu}}{\text{argmin}} (\gamma_{\mu}(t+1) |\phi_{\mu}| + \\ &\quad \frac{1}{2} (\phi_{\mu} - \phi_{\mu}(t+1 \text{ without } L_1))^2) \end{aligned} \quad (\text{S51})$$

$$= \frac{\phi_{\mu}(t+1 \text{ without } L_1)}{|\phi_{\mu}(t+1 \text{ without } L_1)|} \max\{0, |\phi_{\mu}(t+1 \text{ without } L_1)| - \gamma_{\mu}(t+1)\} \quad (\text{S52})$$

$$\gamma_{\mu}(t+1) \equiv \begin{cases} \beta_{\mu}(t+1) \lambda_1 \theta_1 & \text{for } \mu = _i(a_k) \\ \beta_{\mu}(t+1) \lambda_2 \theta_2 & \text{for } \mu = _{ij}(a_k, a_l) \end{cases} \quad (\text{S53})$$

S.1.7.2 L_2 regularization for $\phi_i(a_k)$ and group L_1 for $\phi_{ij}(a_k, a_l)$

The regularization terms of the L_2 for $\phi_i(a_k)$ and the group L_1 for $\phi_{ij}(a_k, a_l)$ are as follows.

$$R \equiv \lambda_1 \sum_i \sum_k \frac{1}{2} \{ \phi_i(a_k)^2 \} + \lambda_2 \sum_i \sum_{j(>i)} \sqrt{\sum_k \sum_l \{ \phi_{ij}(a_k, a_l)^2 \}} \quad (\text{S54})$$

S.1.7.2.1 The soft-thresholding function for group L_1 regularization:

$$\begin{aligned} \phi_{ij}(t+1) &= \text{prox}(\gamma_{ij}(t+1) \|\phi_{ij}\|_2, \phi_{ij}(t+1 \text{ without group } L_1)) \\ &= \underset{\phi_{ij}}{\text{argmin}} (\gamma_{ij}(t+1) \|\phi_{ij}\|_2 + \\ &\quad \frac{1}{2} \|\phi_{ij} - \phi_{ij}(t+1 \text{ without } L_1)\|_2^2) \end{aligned} \quad (\text{S55})$$

$$= \frac{\phi_{ij}(t+1 \text{ without } L_1)}{\|\phi_{ij}(t+1 \text{ without } L_1)\|_2} \max\{0, \|\phi_{ij}(t+1 \text{ without } L_1)\|_2 - \gamma_{ij}(t+1)\} \quad (\text{S56})$$

$$\gamma_{ij}(t+1) \equiv \beta_{ij}(t+1) \lambda_2 \quad (\text{S57})$$

S.1.8 Parameter updates

Given the convexity of the cross entropy function, its minimum can be found by the gradient descent.

S.1.8.1 Modified Adam method (ModAdam)

The modified version of the adaptive learning rate method [62], which is named ModAdam here, has been used.

$$m_\mu(t+1) = \rho_m m_\mu(t) + (1 - \rho_m) \left[\left(\frac{\partial S}{\partial \phi_\mu} \right)_{\phi(t)} \right] \quad (\text{S58})$$

$$v_\mu(t+1) = \rho_v v_\mu(t) + (1 - \rho_v) \left[\left(\frac{\partial S}{\partial \phi_\mu} \right)_{\phi(t)} \right]^2 \quad (\text{S59})$$

$$\kappa(t+1) = \kappa_0 \frac{(1 - \rho_v^{t+1})^{1/2}}{1 - \rho_m^{t+1}} \frac{1}{\max_\mu (v_\mu(t+1)^{1/2}) + \epsilon} \quad (\text{S60})$$

$$\phi_\mu(t+1) = \phi_\mu(t) - \kappa(t+1) m_\mu(t+1) \quad (\text{S61})$$

where κ_0 is an initial learning rate, and ρ_m , ρ_v , and $\epsilon/(1 - \rho_v^{t+1})^{1/2}$ have been set to 0.9, 0.999, and 10^{-8} according to the Adam method [62]. It should be noted here that unlike the Adam method $\kappa(t+1)$ takes the same value for all parameters, because $v_\mu(t+1)^{1/2}$ is replaced by its maximum in Eq. S60.

An important property of Adam's update rule is its careful choice of stepsizes. The effective stepsize is upper bounded by $|\Delta\phi(t+1)| \leq \kappa_0 \max((1 - \rho_m)/\sqrt{(1 - \rho_v)}, 1)$ [62] but essentially all elements of the increment vector $\Delta\phi(t+1)$ are the same order. However, unlike the original Adam, in which $\Delta\phi_\mu(t+1) = -\kappa_0(\sqrt{(1 - \rho_v^{t+1})}/(1 - \rho_m^{t+1}))(m_\mu(t+1)/(v_\mu(t+1)^{1/2} + \epsilon))$, in this modified version the increment $\Delta\phi(t+1)$ is proportional to $-m(t+1)$.

Thus, α_μ and β_μ in Eq. S47 are defined as follows.

$$\alpha_\mu(t+1) = \kappa(t+1) \rho_m m_\mu(t) \quad (\text{S62})$$

$$\beta_\mu(t+1) = \kappa(t+1)(1 - \rho_m) \quad (\text{S63})$$

S.1.8.2 Nesterov's Accelerated Momentum/Gradient method (NAG)

The algorithm of Nesterov's Accelerated Momentum/Gradient method (NAG) [56] employed here is a simple version with the constant friction for velocity as follows. This version includes a correction, which is employed in the Adam method, for the bias that the estimate of the first moment of the gradients will be biased towards zero if it is initialized as zero.

$$m_\mu(t+1) = \rho_m m_\mu(t) + (1 - \rho_m) \left[\left(\frac{\partial S}{\partial \phi_\mu} \right)_{\phi(t)} \right] \quad (\text{S64})$$

$$\phi_\mu(t+1) = \phi_\mu(t) - \kappa_0 [(1 + \rho_m) m_\mu(t+1) - \rho_m m_\mu(t)] \quad (\text{S65})$$

$$= \phi_\mu(t) - \kappa_0 [\rho_m^2 m_\mu(t) + (1 - \rho_m^2) \left(\frac{\partial S}{\partial \phi_\mu} \right)_{\phi(t)}] \quad (\text{S66})$$

$$= \phi_\mu(t) - \kappa_0 [\rho_m m_\mu(t+1) + (1 - \rho_m) \left(\frac{\partial S}{\partial \phi_\mu} \right)_{\phi(t)}] \quad (\text{S67})$$

where κ_0 is an initial learning rate, and ρ_m has been set to 0.95. The α_μ and β_μ in Eq. S47 for the NAG method are defined as follows by replacing $m_\mu(t+1)$ in Eq. S67 by its estimate, $m_\mu(t+1)/(1 - \rho_m^{t+1})$, for the initial condition, $m(0) \equiv 0$.

$$\alpha_\mu(t+1) = \kappa_0 \rho_m^2 [m_\mu(t)/(1 - \rho_m^{t+1})] \quad (\text{S68})$$

$$\beta_\mu(t+1) = \kappa_0 [\rho_m/(1 - \rho_m^{t+1}) + 1] (1 - \rho_m) \quad (\text{S69})$$

S.1.8.3 The number of iterations for learning

The objective function is expected to significantly fluctuate in the minimization process, when the first-order methods based on gradients are employed. In addition, the partial derivatives of Eqs. S40 and S41, which are calculated from the pairwise marginal distributions estimated by Markov Chain Monte Carlo samplings, include statistical errors. Thus, even though the learning rate κ is sufficiently small, the cross entropy/log-likelihood are not monotonically improved. However, the cross entropy/log-likelihood can hardly be evaluated for the Boltzmann machine,

although its partial-derivatives can be easily calculated and then it can be minimized/maximized. Thus, it is not obvious to judge which set of interactions is the best in the learning process.

Here we monitor the average, D_2^{KL} , of Kullback-Leibler divergences for pairwise marginal distributions over all residue pairs as a rough measure of fitting to the reference distribution.

$$D_2^{KL} \equiv \frac{2}{L(L-1)} \sum_i \sum_{j>i} \sum_k \sum_l P_{ij}(a_k, a_l) \log \frac{(P_{ij}(a_k, a_l) + \epsilon)}{(\sum_\sigma P(\sigma) \delta_{\sigma_i a_k} \delta_{\sigma_j a_l} + \epsilon)} \quad (\text{S70})$$

$$D_1^{KL} \equiv \frac{1}{L} \sum_i \sum_k P_i(a_k) \log \frac{(P_i(a_k) + \epsilon)}{(\sum_\sigma P(\sigma) \delta_{\sigma_i a_k} + \epsilon)} \quad (\text{S71})$$

where $\epsilon = 10^{-5}$ is employed to prevent the logarithm of zero. The iteration of parameter updates has been stopped when $\min D_2^{KL}$ over the iteration numbers larger than 1000 does not improve during a certain number, 100, of iterations, and the number of iterations passes over a certain threshold, 1200 iterations. Then the fields and couplings and Monte Carlo samples corresponding to the $\min D_2^{KL}$ over the iteration numbers larger than 1000 are selected.

S.1.9 A gauge employed to compare $h_i(a_k)$ and $J_{ij}(a_k, a_l)$ between various models

The ψ_N of Eq. S4 is invariant under a certain transformation of fields and couplings, $J_{ij}(a_k, a_l) \rightarrow J_{ij}(a_k, a_l) - J_{ij}^1(a_k) - J_{ji}^1(a_l) + J_{ij}^0$, $h_i(a_k) \rightarrow h_i(a_k) - h_i^0 + \sum_{j \neq i} J_{ij}^1(a_k)$ for any $J_{ij}^1(a_k)$, J_{ij}^0 and h_i^0 . Therefore, in order to compare h and J between various models, a certain gauge must be used. Here we use the following gauge that we call the Ising gauge.

$$h_i(\cdot) = \sum_q J_{ij}(a_k, \cdot) = \sum_q J_{ij}(a_q, \cdot) = 0 \quad (\text{S72})$$

where “ \cdot ” denotes the reference state, which is the average over all states for the Ising gauge. Any gauge can be transformed to this gauge by the following transformation.

$$J_{ij}^1(a_k, a_l) \equiv J_{ij}(a_k, a_l) - J_{ij}(\cdot, a_l) - J_{ij}(a_k, \cdot) + J_{ij}(\cdot, \cdot) \quad (\text{S73})$$

$$h_i^1(a_k) \equiv h_i(a_k) - h_i(\cdot) + \sum_{j \neq i} (J_{ij}(a_k, \cdot) - J_{ij}(\cdot, \cdot)) \quad (\text{S74})$$

S.2 FIGURES

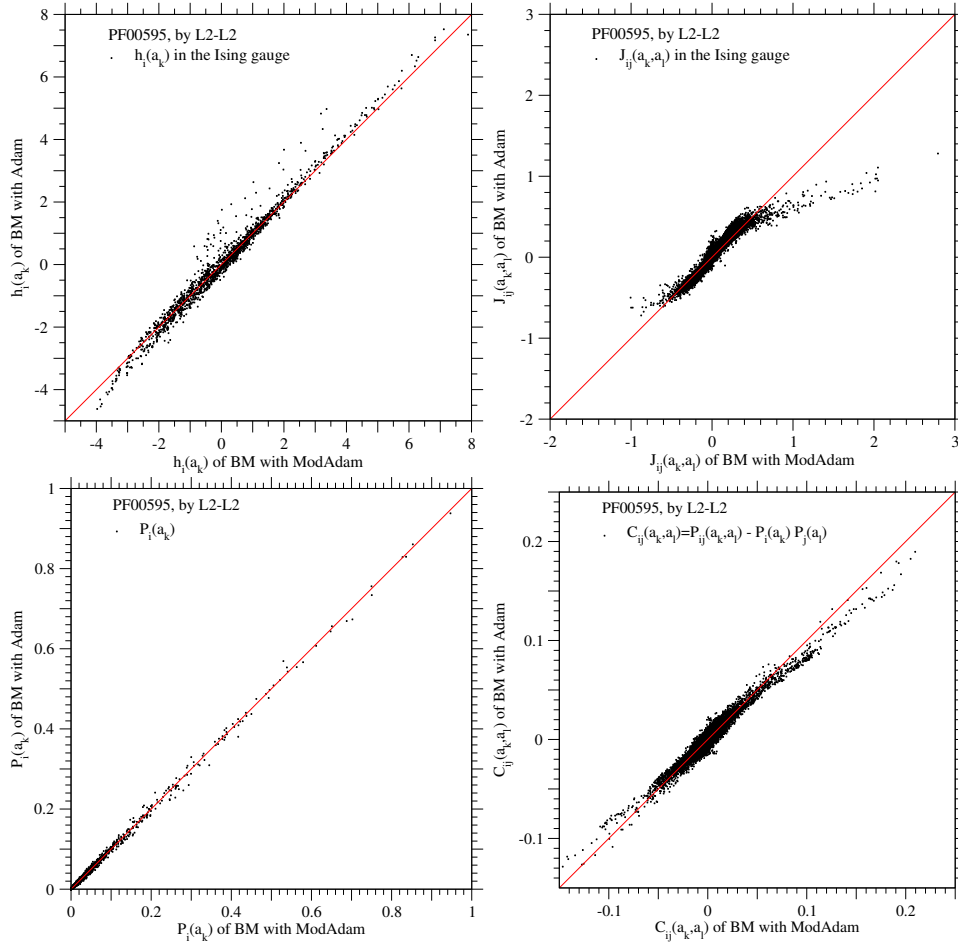


Fig. S1. Comparison of the Adam with the ModAdam gradient-descent method in each of the inferred fields and couplings and the recovered single-site marginals and pairwise correlations for PF00595. The upper left and upper right figures are the comparisons of the inferred fields and couplings in the Ising gauge, respectively, and the lower left and lower right figures are the comparisons of the recovered single-site frequencies and pairwise correlations, respectively. The abscissas and ordinates correspond to the quantities estimated by the modified Adam and Adam methods for gradient descent, respectively. The regularization model L2-L2 is employed for both methods. The solid lines show the equal values between the ordinate and abscissa. The values of hyper-parameters are listed in Table 2. The overlapped points of $J_{ij}(a_k, a_l)$ in the units 0.001 and of $C_{ij}(a_k, a_l)$ in the units 0.0001 are removed.

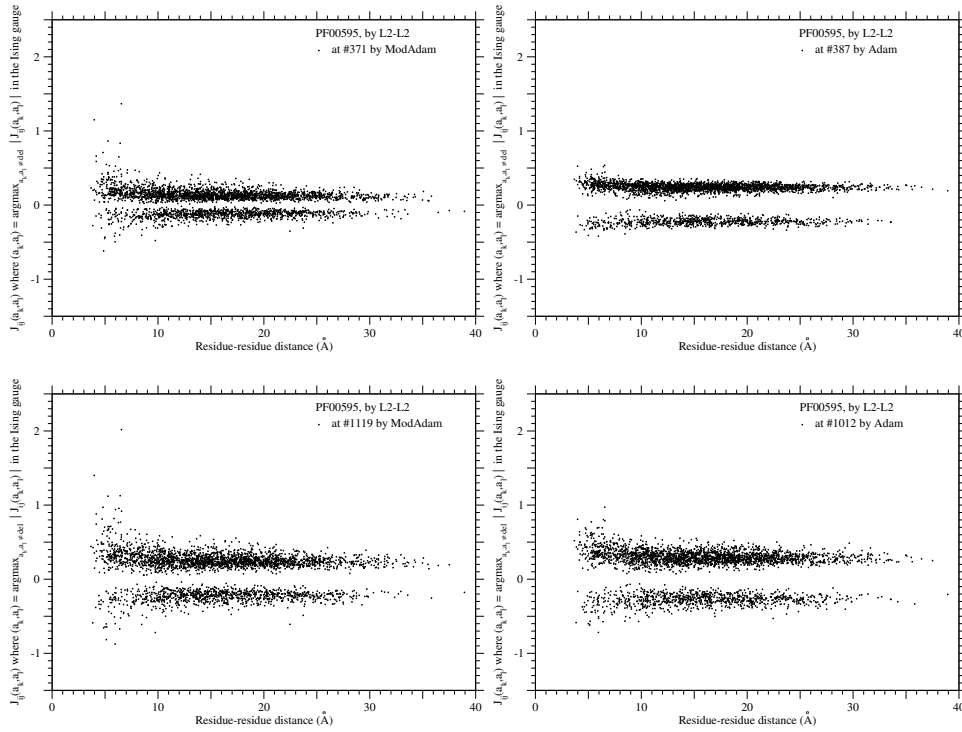


Fig. S2. Differences in the learning of coupling parameters, $J_{ij}(a_k, a_l)$, between the ModAdam and Adam gradient-descent methods for PF00595. All $J_{ij}(a_k, a_l)$ where $(a_k, a_l) = \operatorname{argmax}_{a_k, a_l \neq \text{deletion}} |J_{ij}(a_k, a_l)|$ in the Ising gauge are plotted against the distance between i th and j th residues. The upper left and lower left figures are for the iteration numbers 371 and 1119 in a learning process by the modified Adam method, respectively. The upper right and lower right figures are for the iteration numbers 387 and 1012 in a learning process by the Adam method, respectively. These iteration numbers correspond to $\min D_2^{\text{KL}}$ over the iteration numbers smaller than 400 and those over the iteration numbers larger than 1000. The regularization model L2-L2 is employed for both methods. The learning processes by both methods are shown in Figs. 2 and 5. Please notice that more strong couplings tend to be inferred for closely located residues pairs by the modified Adam method than by the Adam method. The values of hyper-parameters are listed in Table 2.

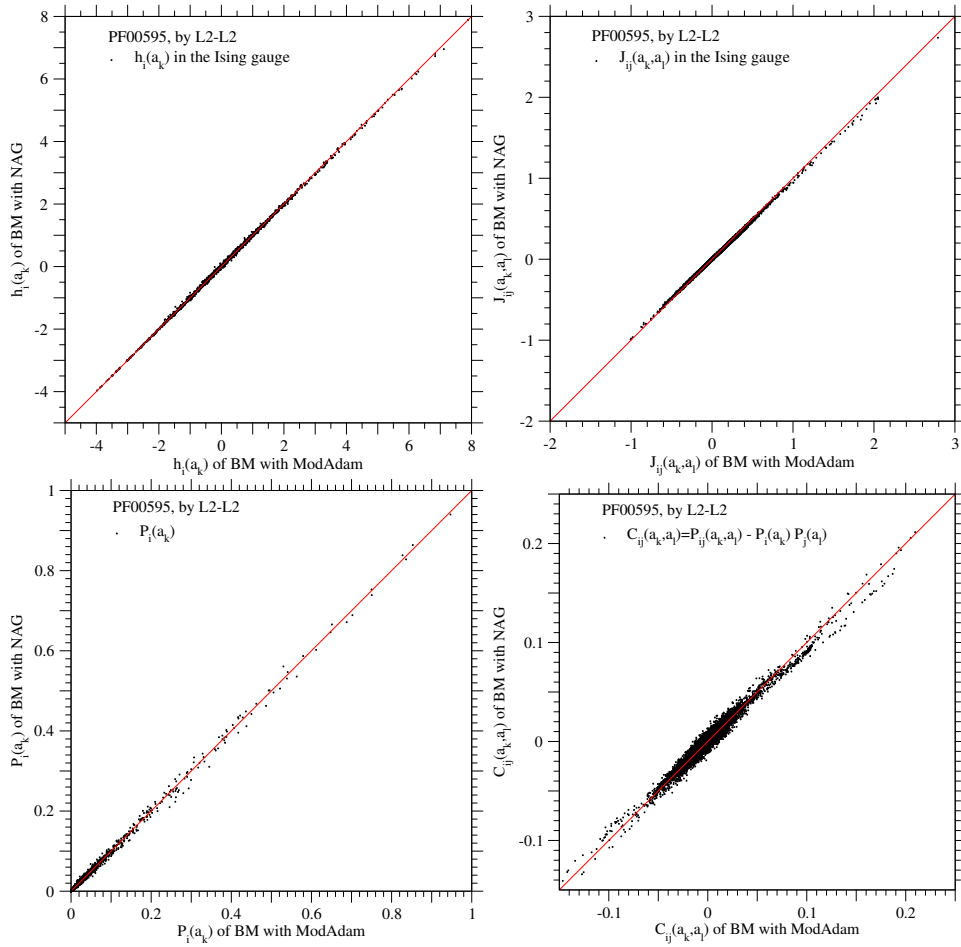


Fig. S3. Comparison of the NAG with the ModAdam gradient-descent method in each of the inferred fields and couplings and the recovered single-site marginals and pairwise correlations for PF00595. The upper left and upper right figures are the comparisons of the inferred fields and couplings in the Ising gauge, respectively, and the lower left and lower right figures are the comparisons of the recovered single-site frequencies and pairwise correlations, respectively. The abscissas and ordinates correspond to the quantities estimated by the modified Adam and NAG methods for gradient descent, respectively. The regularization model L2-L2 is employed for both methods. The solid lines show the equal values between the ordinate and abscissa. The values of hyper-parameters are listed in Table 2. The overlapped points of $J_{ij}(a_k, a_l)$ in the units 0.001 and of $C_{ij}(a_k, a_l)$ in the units 0.0001 are removed.

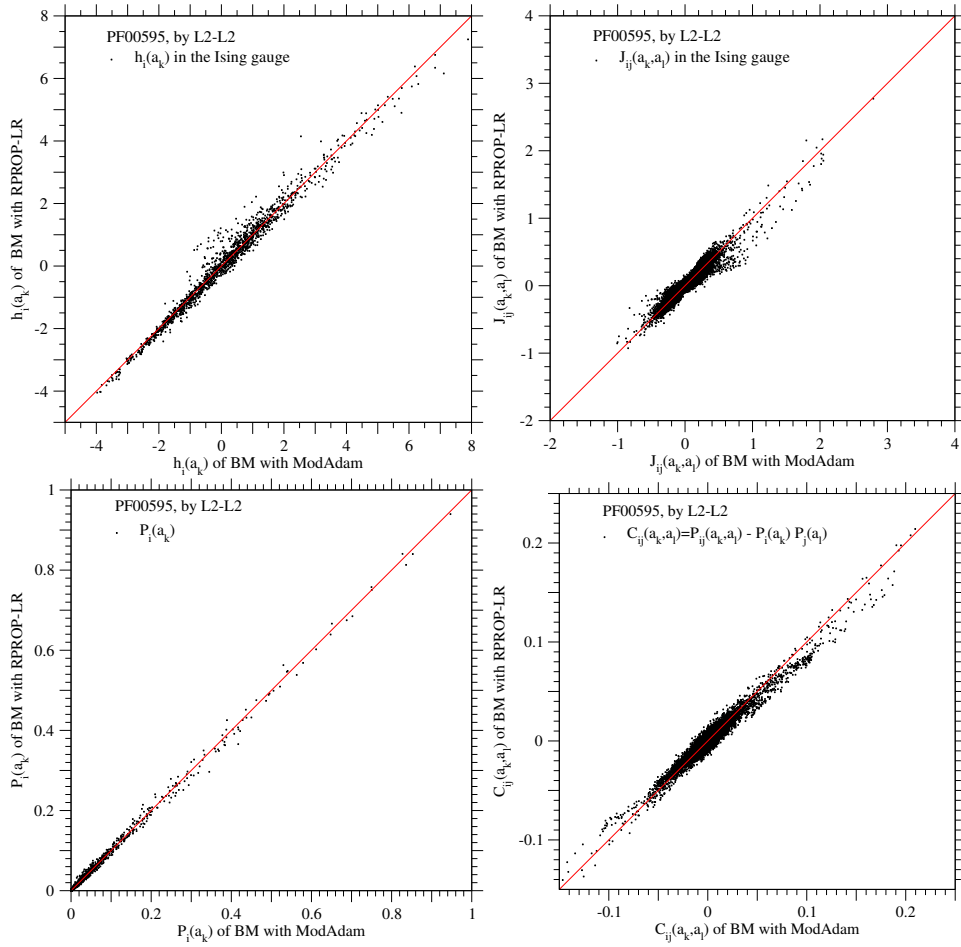


Fig. S4. Comparison of the RPROP-LR with the ModAdam gradient-descent method in each of the inferred fields and couplings and the recovered single-site marginals and pairwise correlations for PF00595. The upper left and upper right figures are the comparisons of the inferred fields and couplings in the Ising gauge, respectively, and the lower left and lower right figures are the comparisons of the recovered single-site frequencies and pairwise correlations, respectively. The abscissas and ordinates correspond to the quantities estimated by the modified Adam and RPROP-LR method for gradient descent, respectively. The regularization model L2-L2 is employed for both methods. The solid lines show the equal values between the ordinate and abscissa. The values of hyper-parameters are listed in Table 2. The overlapped points of $J_{ij}(a_k, a_l)$ in the units 0.001 and of $C_{ij}(a_k, a_l)$ in the units 0.0001 are removed.

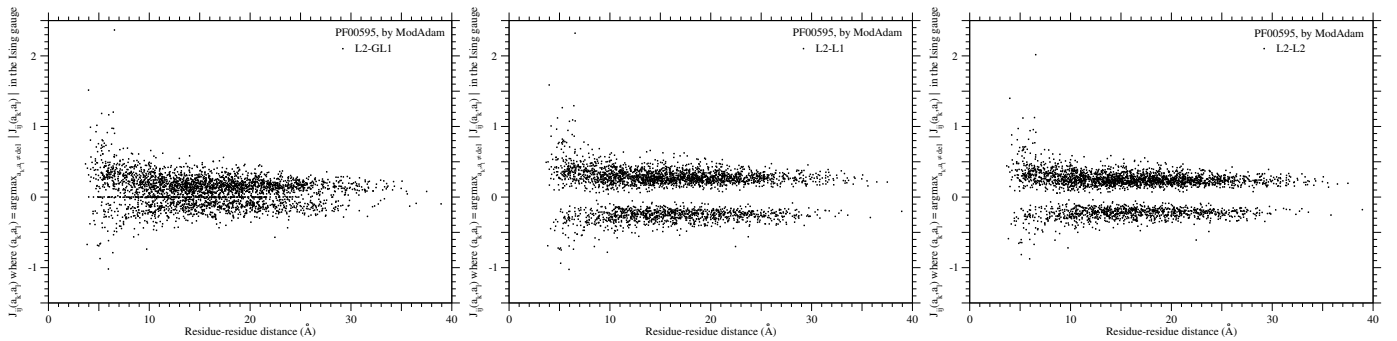


Fig. S5. Differences of inferred couplings J_{ij} among the regularization models for PF00595. All $J_{ij}(a_k, b_l)$ where $(a_k, a_l) = \operatorname{argmax}_{a_k, a_l \neq \text{deletion}} |J_{ij}(a_k, a_l)|$ in the Ising gauge are plotted against the distance between i th and j th residues. The protein family PF00595 is employed. The regularization models L2-GL1, L2-L1, and L2-L2 are employed for the left, middle, and right figures, respectively. The values of regularization parameters are listed in Table 2.

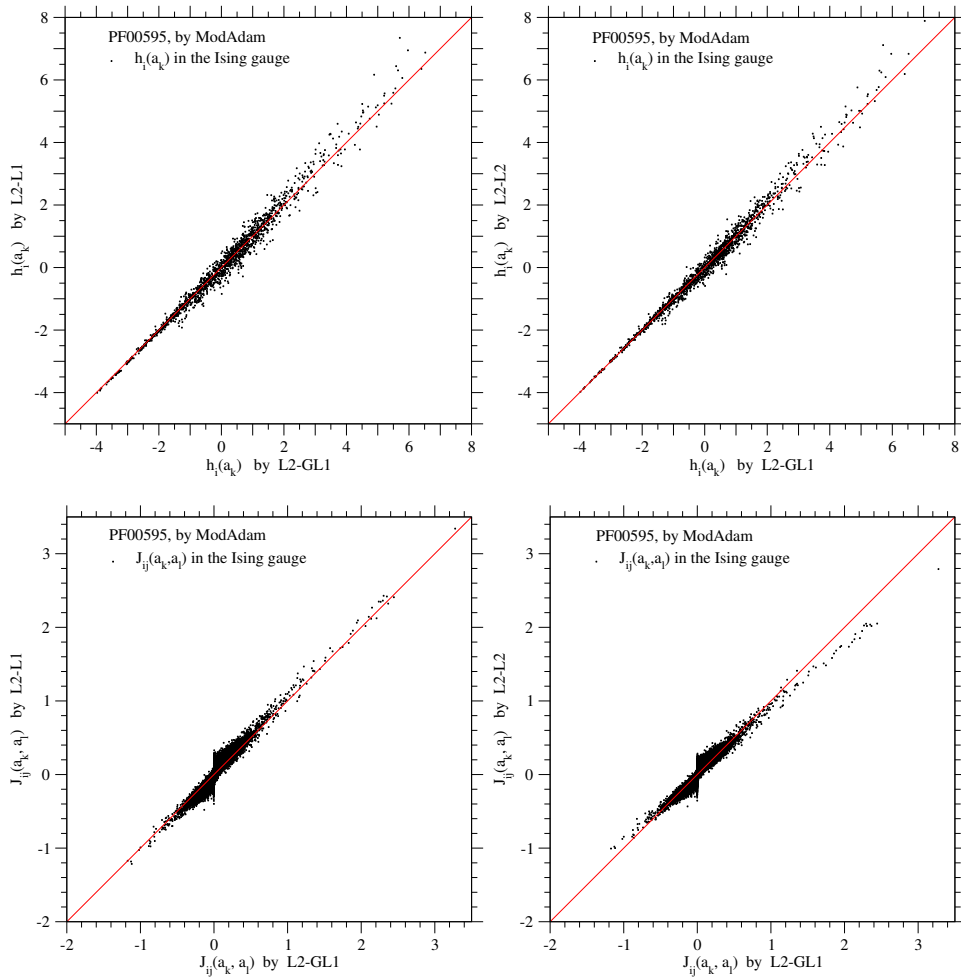


Fig. S6. Comparisons of inferred fields $h_i(a_k)$ and couplings $J_{ij}(a_k, a_l)$ in the Ising gauge between the regularization models for PF00595. The upper and lower figures show the comparisons of fields and couplings in the Ising gauge, respectively. All abscissa correspond to the fields or couplings inferred by the L2-GL1. The ordinates in the left and right figures correspond to the fields or couplings inferred by the L2-L1 and L2-L2 models, respectively. The values of regularization parameters are listed in Table 2. The solid lines show the equal values between the ordinate and abscissa. The overlapped points of $J_{ij}(a_k, a_l)$ in the units 0.001 are removed.

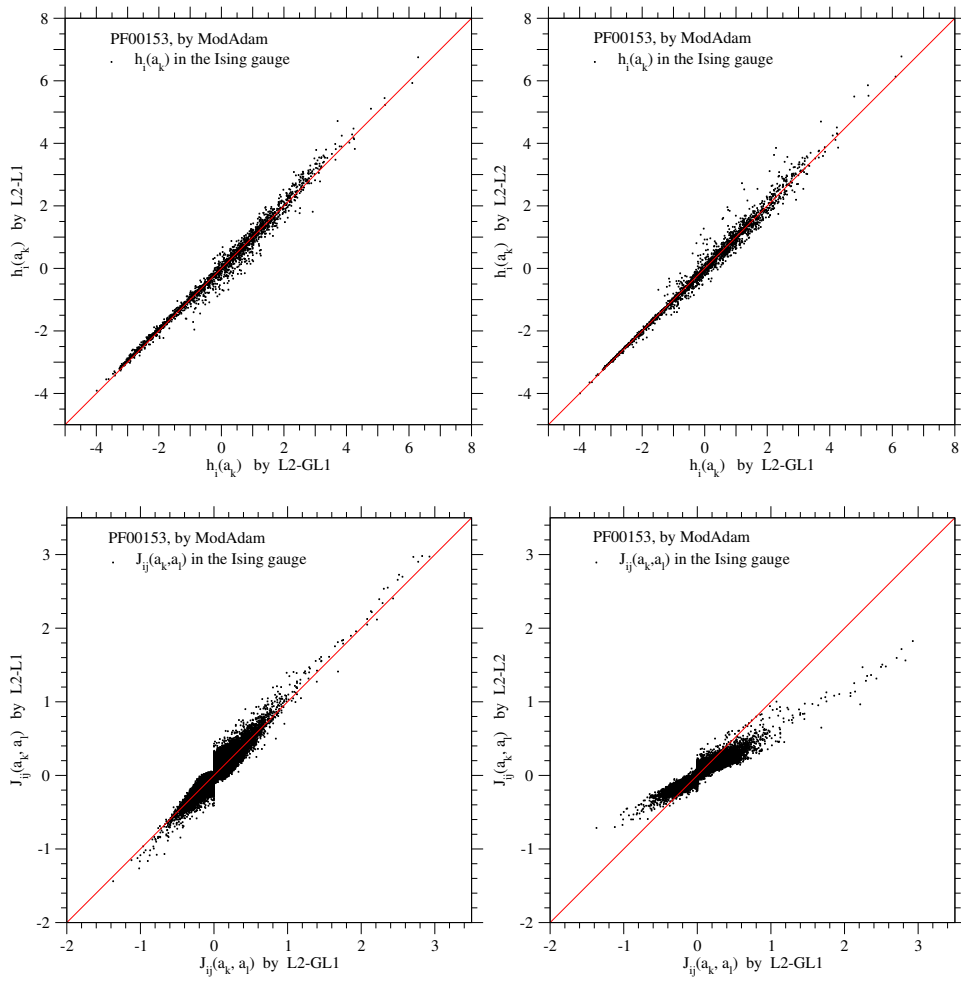


Fig. S7. Comparisons of inferred fields $h_i(a)$ and couplings $J_{ij}(a, b)$ in the Ising gauge between the regularization models for PF00153. The upper and lower figures show the comparisons of fields and couplings in the Ising gauge, respectively. All abscissa correspond to the fields or couplings inferred by the L2-GL1. The ordinates in the left and right figures correspond to the fields or couplings inferred by the L2-L1 and L2-L2 models, respectively. The values of regularization parameters are listed in Table 3. The values of $J_{ij}(a_k, a_l)$ in the units 0.001 are removed.

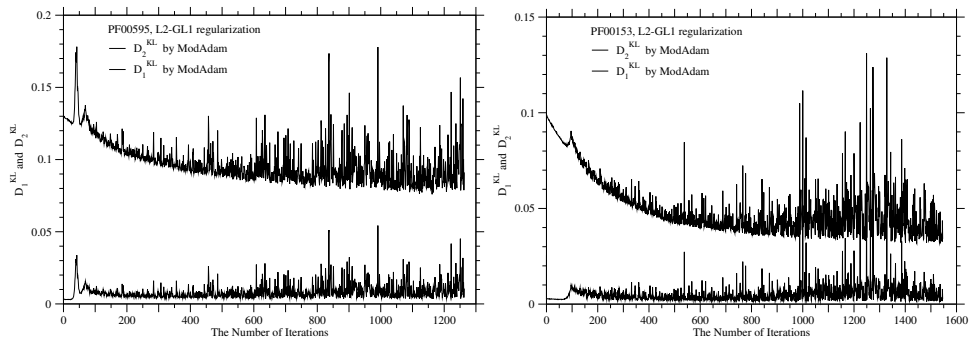


Fig. S8. Learning processes by the L2-GL1 model and the ModAdam method for PF00595 and PF00153. The averages of Kullback-Leibler divergences, D_2^{KL} for pairwise marginal distributions and D_1^{KL} for single-site marginal distributions, are drawn against iteration number in the learning processes with the L2-GL1 model and the ModAdam method for PF00595 and PF00153 in the left and right figures, respectively. The values of hyper-parameters are listed in Tables 2 and 3 as well as others.

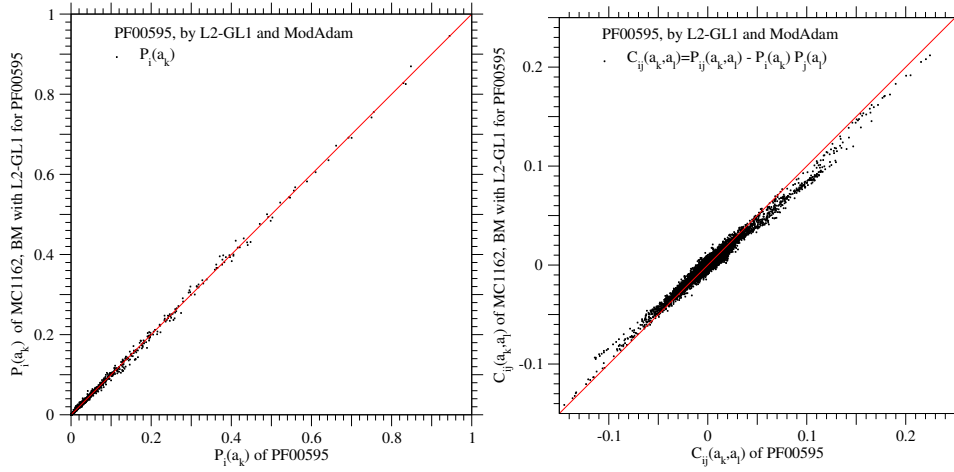


Fig. S9. Recoverabilities of the single-site frequencies and pairwise correlations of PF00595 by the Boltzmann machine learning with the L2-GL1 model and the ModAdam method. The left and right figures are for single-site frequencies and pairwise correlations, respectively; $D_1^{KL} = 0.003695$ and $D_2^{KL} = 0.07594$. The solid lines show the equal values between the ordinate and abscissa. The overlapped points of $C_{ij}(a_k, a_l)$ in the units 0.0001 are removed. See Table 2 for the regularization parameters employed.

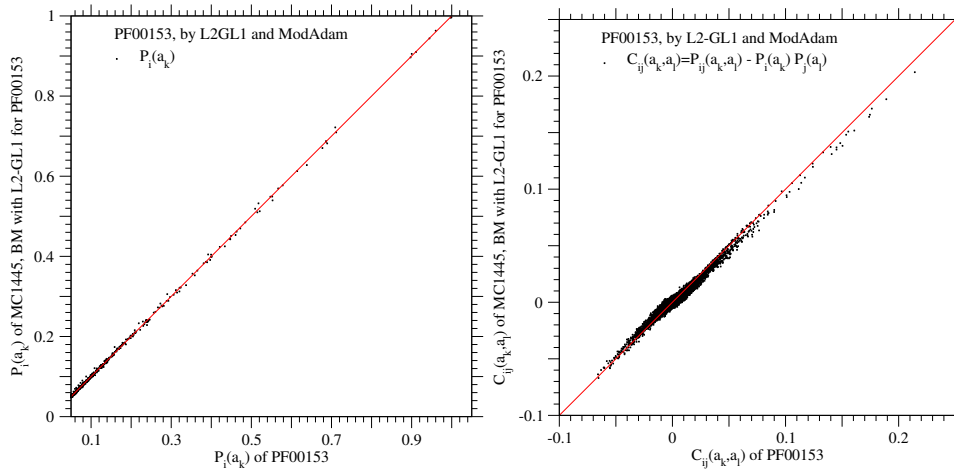


Fig. S10. Recoverabilities of the single-site frequencies and pairwise correlations of PF00153 by the Boltzmann machine learning with the L2-GL1 model and the ModAdam method. The left and right figures are for single-site frequencies and pairwise correlations, respectively; $D_1^{KL} = 0.001120$ and $D_2^{KL} = 0.03176$. The solid lines show the equal values between the ordinate and abscissa. The overlapped points of $C_{ij}(a_k, a_l)$ in the units 0.0001 are removed. See Table 3 for the regularization parameters employed.

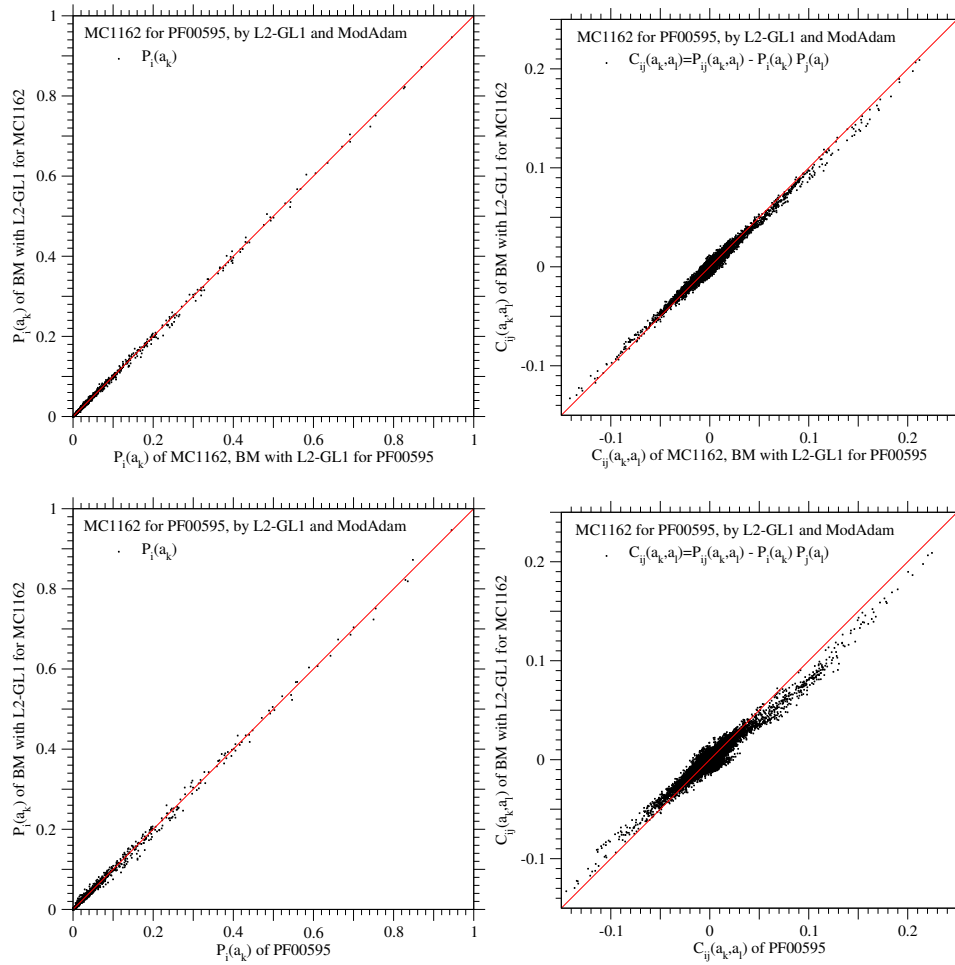


Fig. S11. Recoverabilities of the single-site frequencies and pairwise correlations by the Boltzmann machine learning with the L2-GL1 model and the ModAdam method for the protein-like sequences, the MCMC samples that are obtained by the same Boltzmann machine for PF00595. The MCMC samples obtained by the Boltzmann machine learning with the L2-GL1 model and the ModAdam method for PF00595 are employed as protein-like sequences for which the Boltzmann machine learning with the same model and method is executed again in order to examine how precisely the marginals of the protein-like sequences can be recovered. The marginals recovered by the Boltzmann machine learning for the MCMC samples are compared to those of the MCMC samples in the upper figures, and to those of PF00595 in the lower figures. The left and right figures are for the single-site probabilities and pairwise correlations, respectively. The solid lines show the equal values between the ordinate and abscissa. The overlapped points of $C_{ij}(a_k, a_l)$ in the units 0.0001 are removed. See Table 2 for the regularization parameters employed.

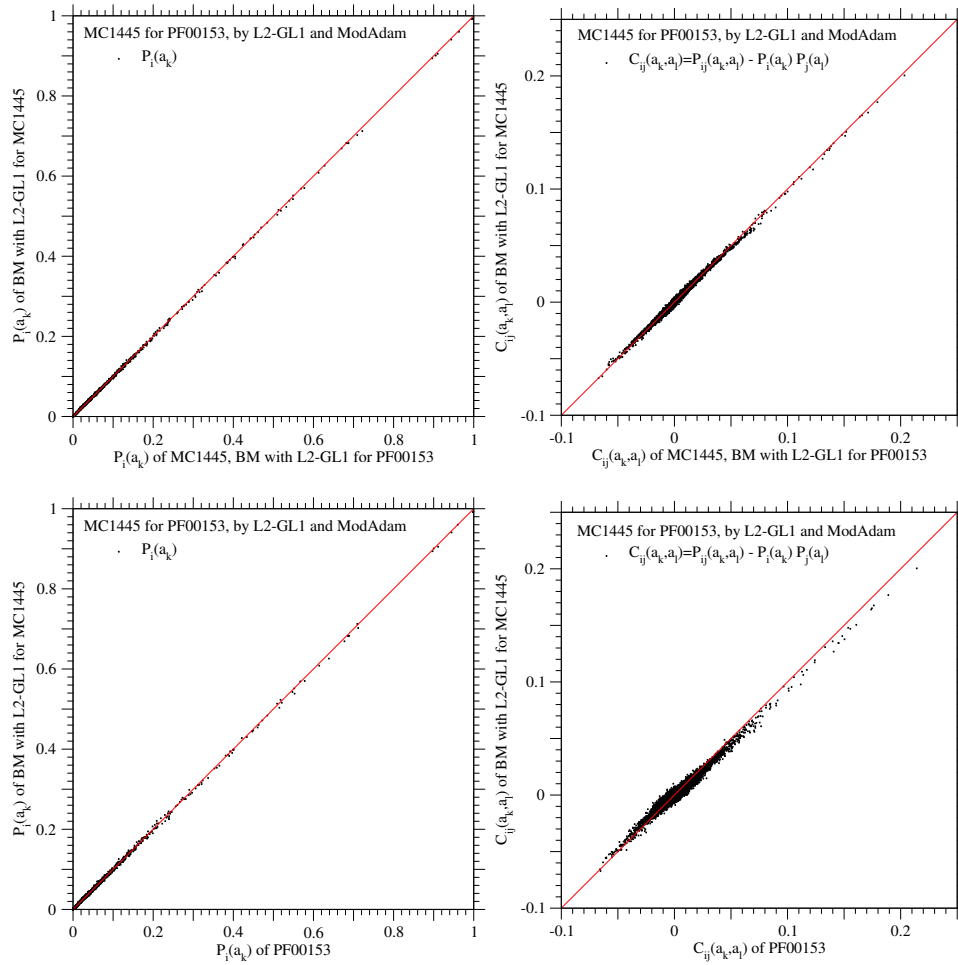


Fig. S12. Recoverabilities of the single-site frequencies and pairwise correlations by the Boltzmann machine learning with the L2-GL1 model and the ModAdam method for the protein-like sequences, the MCMC samples that are obtained by the same Boltzmann machine for PF00153. The MCMC samples obtained by the Boltzmann machine learning with the L2-GL1 model and the ModAdam method for PF00153 are employed as protein-like sequences for which the Boltzmann machine learning with the same model and method is executed again in order to examine how precisely the marginals of the protein-like sequences can be recovered. The marginals recovered by the Boltzmann machine learning for the MCMC samples are compared to those of the MCMC samples in the upper figures, and to those of PF00153 in the lower figures. The left and right figures are for the single-site probabilities and pairwise correlations, respectively. The solid lines show the equal values between the ordinate and abscissa. The overlapped points of $C_{ij}(a_k, a_l)$ in the units 0.0001 are removed. See Table 3 for the regularization parameters employed.